NAVAL POSTGRADUATE SCHOOL

MONTEREY, CALIFORNIA

THESIS

THERMO-MECHANICAL RESPONSE OF MONOLITHIC AND NiTi SHAPE MEMORY ALLOY FIBER REINFORCED Sn-3.8Ag-0.7Cu SOLDER.

by

Evangelos Fountoukidis

September 2005

Thesis Advisor: Indranath Dutta

Approved for public release; distribution is unlimited

THIS PAGE INTENTIONALLY LEFT BLANK

REPORT DOCUMENTATION PAGE			*Form Approved OMB No. 0704-0188*
Public reporting burden for this collection of information is estimated to average 1 hour per response, including the time for reviewing instruction, searching existing data sources, gathering and maintaining the data needed, and completing and reviewing the collection of information. Send comments regarding this burden estimate or any other aspect of this collection of information, including suggestions for reducing this burden, to Washington headquarters Services, Directorate for Information Operations and Reports, 1215 Jefferson Davis Highway, Suite 1204, Arlington, VA 22202-4302, and to the Office of Management and Budget, Paperwork Reduction Project (0704-0188) Washington DC 20503.			
1. AGENCY USE ONLY *(Leave blank)*	**2. REPORT DATE** September 2005	**3. REPORT TYPE AND DATES COVERED** Master's Thesis	
4. TITLE AND SUBTITLE: Thermo-Mechanical Response of Monolithic and NiTi Shape Memory Alloy Fiber Reinforced Sn-3.8Ag-0.7Cu Solder.			**5. FUNDING NUMBERS**
6. AUTHOR(S) Evangelos Fountoukidis			
7. PERFORMING ORGANIZATION NAME(S) AND ADDRESS(ES) Naval Postgraduate School Monterey, CA 93943-5000			**8. PERFORMING ORGANIZATION REPORT NUMBER**
9. SPONSORING /MONITORING AGENCY NAME(S) AND ADDRESS(ES) N/A			**10. SPONSORING/MONITORING AGENCY REPORT NUMBER**
11. SUPPLEMENTARY NOTES The views expressed in this thesis are those of the author and do not reflect the official policy or position of the Department of Defense or the U.S. Government.			
12a. DISTRIBUTION / AVAILABILITY STATEMENT Approved for public release; distribution is unlimited			**12b. DISTRIBUTION CODE**
13. ABSTRACT (maximum 200 words) In electronic packaging, the reliability of solders is a critical issue, since serve as both electrical and mechanical connections. The most common failures arise from the thermo-mechanical fatigue (TMF) of solders, due to mismatches in the coefficient of thermal expansion between the Si-chip and the printed circuit board. In order to meet the demands of miniaturization and enhanced performance in severe environments, a novel adaptive Tin-Silver-Copper (SnAgCu) solder reinforced with NiTi shape-memory alloy (particles or fiber) developed. An experimental apparatus has been designed to investigate the thermo-mechanical strain-controlled fatigue life of the solder during both single and multiple thermal cycling under double-shear loading. For comparison, thermo-mechanical single shear tests were also performed in monolithic Tin-Silver-Copper solder and in solder reinforced with Cu fiber. Also, micro-structural evaluation of the solders during the 5th cycle was possible using Scanning and Optical microcopy together with EDS analysis.			
14. SUBJECT TERMS Shape Memory Alloy, Thermo-mechanical Cycling, Low-cycle Fatigue, Shape Memory Effect, Nickel Titanium Solder			**15. NUMBER OF PAGES** 89
			16. PRICE CODE
17. SECURITY CLASSIFICATION OF REPORT Unclassified	**18. SECURITY CLASSIFICATION OF THIS PAGE** Unclassified	**19. SECURITY CLASSIFICATION OF ABSTRACT** Unclassified	**20. LIMITATION OF ABSTRACT** UL

THIS PAGE INTENTIONALLY LEFT BLANK

Approved for public release; distribution is unlimited

THERMO-MECHANICAL RESPONSE OF MONOLITHIC AND NiTi SHAPE MEMORY ALLOY FIBER REINFORCED Sn-3.8Ag-0.7Cu SOLDER.

Evangelos Fountoukidis
Lieutenant, Hellenic Navy
B. S., Hellenic Naval Academy, 1992

Submitted in partial fulfillment of the
requirements for the degree of

MASTER OF SCIENCE IN MECHANICAL ENGINEERING

from the

**NAVAL POSTGRADUATE SCHOOL
September 2005**

Author: Evangelos Fountoukidis

Approved by: Indranath Dutta
                  Thesis Advisor

                  Anthony J. Healey
                  Chairman, Department of Mechanical and
                  Astronautical Engineering

iii

THIS PAGE INTENTIONALLY LEFT BLANK

ABSTRACT

In electronic packaging, the reliability of solders is a critical issue, since serve as both electrical and mechanical connections. The most common failures arise from the thermo-mechanical fatigue (TMF) of solders, due to mismatches in the coefficient of thermal expansion between the Si-chip and the printed circuit board. In order to meet the demands of miniaturization and enhanced performance in severe environments, a novel adaptive Tin-Silver-Copper (SnAgCu) solder reinforced with NiTi shape-memory alloy (particles or fiber) developed.

An experimental apparatus has been designed to investigate the thermo-mechanical strain-controlled fatigue life of the solder during both single and multiple thermal cycling under double-shear loading. For comparison, thermo-mechanical single shear tests were also performed in monolithic Tin-Silver-Copper solder and in solder reinforced with Cu fiber. Also, micro-structural evaluation of the solders during the 5th cycle was possible using Scanning and Optical microcopy together with EDS analysis.

THIS PAGE INTENTIONALLY LEFT BLANK

TABLE OF CONTENTS

THIS PAGE INTENTIONALLY LEFT BLANK

LIST OF FIGURES

LIST OF TABLES

THIS PAGE INTENTIONALLY LEFT BLANK

ACKNOWLEDGMENTS

The author is grateful to Professor Indranath Dutta for his guidance and continued support during the evolution of this research.

I would also like to thank my wife Chrysoula, who patiently understood and supported me during the completion of the thesis.

THIS PAGE INTENTIONALLY LEFT BLANK

I.   INTRODUCTION

A.   SOLDERS IN ELECTRONICS

In electronics technology, the assembly of electronic circuits is critically dependent on the use of the solders. Aside from the primary role of serving as reliable electrical interconnections, circuits serve a crucial mechanical role. They also have to provide structural integrity, particularly in surface-mount technology applications. Therefore, the mechanical properties of the solders are important, since their failure can affect the integrity of the structural assembly.

The present miniaturization trend toward higher-performance, smaller and lighter products have resulted in an increasing demand for smaller component packages and/or higher pin counts. According to the Semiconductor Industry Association Roadmap, the number of input/output (I/O) interconnects in integrated circuits is expected to significantly increase over the next 10 years.

The Quad Flat Pack (QFP) and the Ball Grid Array (BGA) packages today both offer a large number of I/Os, as required by modern integrated circuit (IC) technology. The BGA concept has received a great deal of attention, owing to its inherent, potential benefits to surface mount production. In order to accommodate the increasing number of I/Os needed, the peripheral QFP technology is forced to an ever-finer lead pitch, with thinner and more fragile leads. The BGA, taking advantage of the area under the package for the solder-sphere interconnections, satisfies the I/O demand using a far coarser pitch. Additionally, the package size and the board real estate required are usually smaller for BGA packages; they are less fragile and easier to handle, both before and during assembly.

In actual flip-chip application, the BGA's solder balls may initially be placed on the printed circuit board (PCB) and the chip placed precisely over the BGA. The system then passes through a furnace that melts the solder and provides permanent connection between the BGA and the PCB. For lower pin counts, most often a two-sided substrate metallization is sufficient to provide

1

electrical contact from wire-bonds through-holes to solder ball pads. In addition, thermal balls under the center of the package are often used to remove heat from the device through thermal vias. These BGAs are illustrated in Figure1.
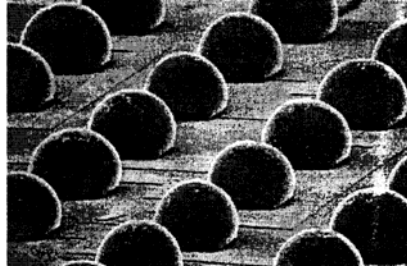
Figure 1.   Solder bumps on a wafer, from reference [1]

A cross-section of a BGA is shown in Figure 2, depicting the over-molded and wire-bonded chip, attached to the BT carrier (sometimes FR-4) substrate, the other side of which is attached to the solder balls responsible for the final interconnection to the printed circuit board.
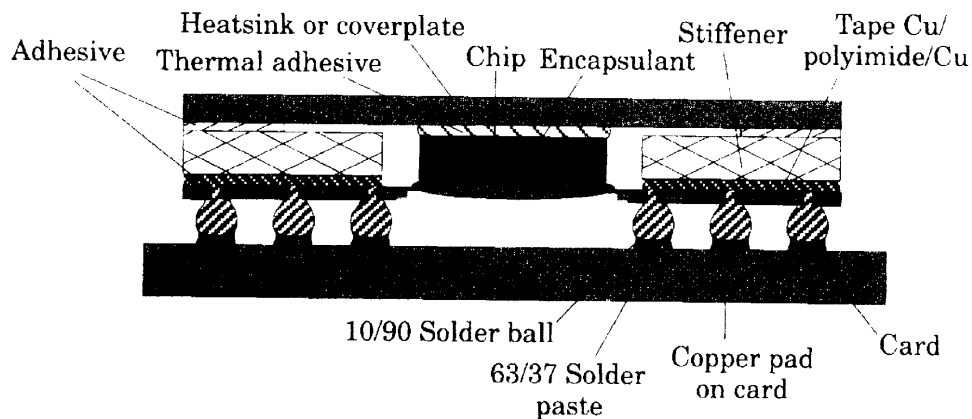
Figure 2.   Cross section of a Ball Grid Array (BGA), from reference [6]

For interconnection and packaging, Pb-Sn and eutectic 63Sn-37Pb solders have been widely used in the past for low cost, ease of manufacturability

and good wettability on common electronic component substrates such as Cu and Ni. These low-cost tin-lead solders have been used as joining materials in electronics for many years, and have fueled creative advanced-packaging developments such as solder-bumped flip chips, ball grid array (BGA) packages and chip scale packages (CSP). For these packaging technologies, the tin-lead solders, applied as tiny solder balls, were the electrical and mechanical glue of the printed circuit board (PCB) assemblies.

However, there were environmental and health issues concerning the toxicity of Pb present in this Sn-Pb solder alloys—as well as a need for solder with various melting temperatures for use in hierarchical electronic structures-- that inspired the use of lead-free substitute alloys.

With the drive toward lead-free products, one of the challenges was to find an alternative solder alloy that was as cost effective, manufacturable, available and reliable as the industry standard eutectic tin-lead or high-lead solders. Now, eutectic Sn-Ag-Cu (SAC) or Sn-3.5Ag is recognized as the standard lead-free solder alloy for packaging interconnects in the electronics industry.

B.   PERFORMANCE AND RELIABILITY ISSUES OF THE SOLDERS

In service, solders experience complex loading conditions, such as creep and fatigue, under several possible modes, including tension, shear and torsion. More precisely, during thermal cycling conditions as an electronic system is placed in operation, thermal mismatch deformations arise due to differences in the coefficient of thermal expansion (CTE) between the Si-chip and the printed circuit board (PCB).

Table 1 gives the CTE of some common materials which often used in the Electronic Package Technology.

Material	CTE $(10^{-6}/K)$
FR-4 (PCB material)	11-15
Epoxies	60-80
Sn-37Pb	21
Sn-3.5Ag	22
Sn-20In-2.8Ag	28

Table 1. CTE date for various components in Electronic Packaging, from reference [7-10]

Although lead-free solders are now in use, reliability issues still exist from this high thermal mismatch deformation, resulting in large solder-joint stresses and strains and causing fatigue failure. The solder balls experience a combination of creep and cyclic shear deformation, and this leads to failure of the solder at locations where the inelastic strain range is highest, typically near the Si substrate [1].

A schematic illustration of the shear that develops in a solder joint between a chip and substrate when the device is heated by operating current or a change in ambient temperature is given in Figure 3.
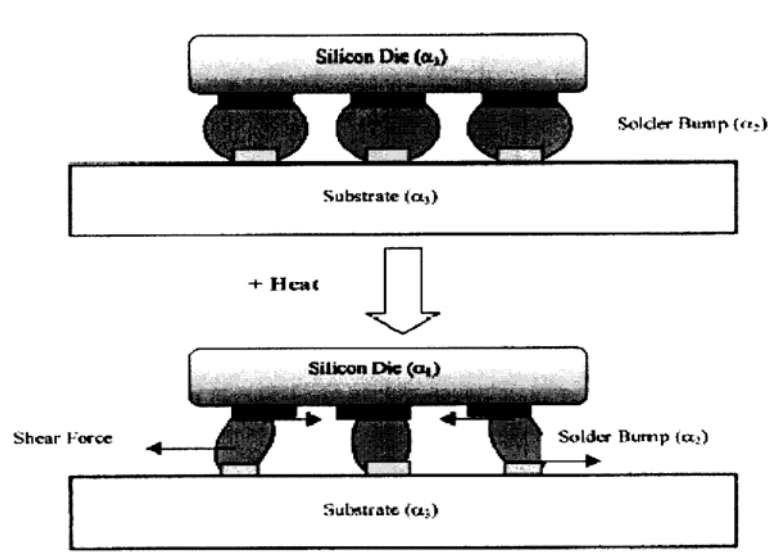
Figure 3.   Thermally induced stress during normal operation, from reference [13]

Also, as lead-free solders operate at high homologous temperatures, higher than 0.8, coarsening of the eutectic structure can occur with time, and this is enhanced in regions of strain localization. These high strain ranges lead to thermo-mechanical failure of the solder, as they greatly influence its fatigue life. In addition, for the SnAgCu solders the formation and growth of intermetallic compounds (IMC) between solder and substrate can have a detrimental effect on the solder's life, as this region is extremely brittle. The developing of one such crack can be seen in Figure 4.
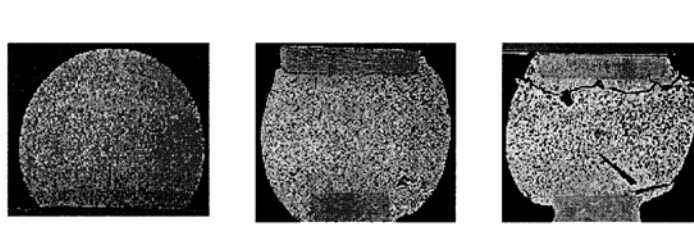
Figure 4.   Crack region of SnAgCu solder after TMF, from reference [1]

C.   HIGH-PERFORMANCE LEAD-FREE COMPOSITE SOLDERS

Lead-free solders, such as the eutectic 96.5Sn/3.5Ag or the Sn-Ag-Cu with variable composition, exhibit high strength and higher melting points (221°C and 217°C, respectively) compared with tin-lead eutectic solder. Also, it was determined that SnAgCu represents a better choice over the other leading candidates to replace tin-lead, in terms of temperature physical characteristics, fatigue resistance and grain-structure phase stability.

Furthermore, developments resulting in "composite solders" utilized an intermetallic or metallic compound interspersed in a solder matrix.   The mechanical properties of this composite solder were found to be superior to those of standard tin/silver solder. Specifically, they improved the strength and

creep resistance of solder by retarding grain-boundary sliding, impeding grain growth and redistributing stresses uniformly.

Research on the use of shape-memory alloys (SMAs) in composites has been gaining momentum over the past few years. SMAs, when in the form of wires, short fibers or particulates, can be embedded into a host material to form a SMA composite. In this scheme, the SMA reinforcement deforms in shear concurrently with the solder during TMC as they undergo martensite-to-austenite transformation, while the solder matrix nearest to the reinforcement is put in reverse shear.

The purpose of this thesis is to study the thermo-mechanical response behavior of a 96.5Sn-3.8Ag-0.7Cu lead-free composite solder, reinforced with NiTi shape-memory alloy (SMA) fiber and ribbon, during thermal cycling under shear loading. The behavior of the NiTi reinforced solder, will be compared with monolithic and Cu (passive) reinforced solders. During TMC, the SMA fiber, is expected to reduce the inelastic strain concentrations within the solder joints via internal self-actuation at the A_s (Austenite starting transformation) temperature. Also, an evaluation of the microstructure of the solders and the development of a method to produce eutectic solder reinforced with NiTi powder is presented.

II.   BACKGROUND

A.   DEVELOPMENTS IN SOLDERS OF ELECTRONIC COMPONENTS

1.   General

Soldering is a well-known metallurgical joining method using a filler metal (the solder) with a melting point below $425^{o}C$ to $137^{o}C$. To form a proper metallurgical bond between two metals, wetting must takes place. This means that a specific interaction must take place between liquid solder and the solid surfaces of the parts to be soldered. Solders can be classified as soft and hard. Soft solders are characterized by melting temperatures below about $190^{o}C$, while hard solders melt between $190^{o}C$ and $425^{o}C$ [2].

2.   Tin-Lead Solders

With a melting temperature of $183^{o}C$, the tin-lead binary system allows soldering conditions that are compatible with most substrate materials and Surface Mount Technology (SMT) devices. As one of the primary components of eutectic solders, lead imparts many technical advantages to tin-lead solders, including reduction of the surface tension of pure tin (550 dyne/cm at $232^{o}C$); the lower surface tension of the composite solder (470dyne/cm 63Sn-37Pb at 280-$176^{o}C$) facilitates wetting [3]. Also, lead serves as a solvent metal, enabling the other joint constituents, such as Sn and Cu, to form intermetallic bonds rapidly [4].

There exists a relatively well-established knowledge base about the physical metallurgy, mechanical properties, flux chemistries, manufacturing processes and reliability of eutectic tin-lead solders [8, 9, and 10]. SMT assembly and soldering equipment was engineered almost exclusively with tin-lead solder in mind. A good understanding of the behavior of tin-lead solders has enabled current SMT technology to assemble and create small-geometry solder joints (approaching 75 microns in size), in high volume and at a competitive cost.

3.   Lead-Free Solders

However, the lead that is contained in these solders is toxic and can affect human health and create environmental problems in combination with trade and

legislative issues [20]. Because of this background, lead-free solders require further development, and their metallurgical properties should be comparable to Sn-Pb solder alloys. Therefore, studies of lead-free solder alloys, evaluation of their mechanical properties, measurements of their melting points and evaluations of their wettability on base metal are still being performed [5,7].

Current manufacturing technologies are based upon the 183°C melting point of the near-eutectic 40Pb-60Sn, and the search for a suitable lead-free solder alloy with an equivalent melting point has posed a considerable challenge. The best possible solution would be the creation of a solder alloy that not only had the same characteristics as Pb-Sn, but also had equivalent or better properties with respect to wetting, strength, creep and fatigue resistance [6, 20].

One popular alloy, which The National Electronics Manufacturing Initiative (NEMI) chooses as the sequencer of the lead alloys, is the Sn-Ag-Cu ternary alloy system, because it contains elements common to those already in use in current soldering technology [7]. The binary Sn-Ag (whose eutectic temperature is 221°C) depresses the liquidus temperature by the addition of Cu in an effort to make Sn-Ag base alloys more compatible with tin-lead manufacturing procedures [11]. Figure 5 demonstrate the phase diagram together with the predicted composition of the eutectic solder.
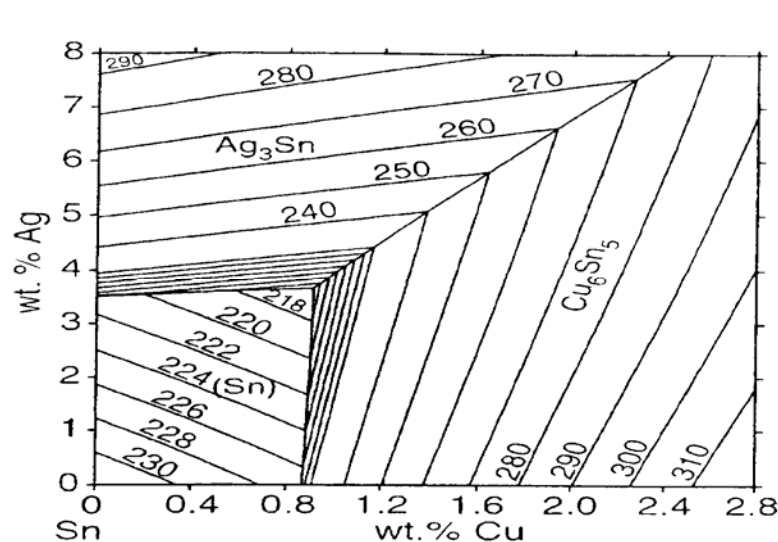
Figure 5.   Phase diagram of 95.5Sn-3.8Ag-0.7Cu solder, from reference [20]

4. Composite Solders

Furthermore, the composite approach was adopted in solder research in the past few years by use of dispersion-strengthening (DS) solders. In an effort to improve the comprehensive properties of bulk solders and their soldered joints, this method has shown that certain composite solders have exhibited enhanced strength and other desired properties such as creep resistance and fatigue life [12, 13, 14 and 15].

Additions of metallic particles to form intermetallic phases in the solder matrix have been the main focus of the composite approach. An important consideration is that the modified solder should function similarly to monolithic solder by appropriately demonstrating good wetting of the substrate, proper flow characteristics and reliable bonding [23]. These metallic particles are mostly commercially available, micro-sized particles [16, 17]. The mechanical dispersion of fine particles (metallic or intermetallic) has been proven through mechanical methods of both introduction to paste material and molten solder. These particles are carefully chosen to ensure that they are uniformly distributed within the solder [18, 19].

Composite solder with SnAgCu matrix, via an in situ process, causes the creation of Cu_6Sn_5 dispersions and forms a more uniform and thinner intermetallic layer at the solder/Cu contact pad interface. The average thickness was about one half that of eutectic solder after three evolutions of reflow soldering. The dispersions were, however, found to coarsen very significantly during the reflow processing and their gravitational sedimentation was observed [21].

Marshall et al [22] developed a composite solder using an intermetallic as the filler in a tin-lead matrix, one whose micro-structural analysis, combined with the apparent increase of the mechanical properties, indicates that it may prove to be a superior material in appropriate applications. Actually, propagation of cracks typically did not occur along, or in contact with, the intermetallic particles, and in

the instances where crack propagation terminated at a particle, the crack did not continue through the particle.

Subramanian et al [23] observed the fracture behavior of a composite eutectic Sn-Ag solder containing 20% Volume fraction Cu_6Sn_5 during thermo-mechanical service. The strain was delocalized in the specimen as a whole as a result of a uniform cracking, resulting in a ductile, Mode I fracture behavior. These can directly affect the resistance of the solder to creep and thermo-mechanical fatigue.

Furthermore, the eutectic solders bond strongly with Cu substrate by forming intermetallic layers between the solder and the Cu substrate. However, these layers tend to grow with time by solid-state diffusion even at ambient temperatures. They can be sources of mechanical weakness in solder joints due to the brittle nature of the intermetallics, or can cause delamination at the interface [25]. But the presence of the intermetallic reinforcements retards the growth of the interface intermetallic layer, even at long aging times [24].

Finally, in situ dispersions in the solder have been observed to decrease the strain-controlled fatigue life, cause more rapid creep-damage accumulation and, because of its greater strength and stiffness, the composite solder may subject the brittle semiconductor device to larger stresses that are generally desirable [26].

5. Solders Reinforced by Shape-Memory Alloys (NiTi)

From the above, it is clear that solders with "passive" reinforcements have provided some improvements in stress-controlled fatigue life, but have not shown the needed improvements in thermo-mechanical fatigue life under strain-controlled conditions, which is a primary deformation mode in such applications. Therefore, conventional particle strengthening of solder causes many reliability problems during an aggressive thermo-mechanical cycling on service conditions [5].

In response to these problems, there has arisen considerable interest in developing adaptive solder alloys reinforced by a small amount of NiTi shape-memory alloy (SMA) particles or fiber.

The term shape-memory alloys is applied to that group of metallic materials that demonstrate the ability to return to some previously defined shape or size when subjected to the appropriate thermal procedure. Generally, these materials can be plastically deformed at some relatively low temperature, and upon exposure to some higher temperature will return to their shape prior to the deformation. Materials that exhibit shape memory only upon heating are referred to as having a one-way shape memory. Some materials also undergo a change in shape upon recooling. These materials have a two-way shape memory [34].

The first recorded observation of the shape-memory transformation was in the 1930s. In 1938, the transformation was seen in brass (copper-zinc); however, it was not until 1962 that the effect was discovered in equiatomic nickel-titanium (Ni-Ti). As the shape-memory effect became better understood, a number of other alloy systems that exhibited shape memory were investigated [34].

Although a relatively wide variety of alloys are known to exhibit the shape-memory effect, only those that can recover substantial amounts of strain or that generate significant force upon changing shape are of commercial interest. To date, these have been the nickel-titanium alloys and copper-base alloys. In particular, the NiTi alloys have greater shape-memory strain (up to 8%), tend to be thermally stable and have excellent corrosion resistance [34].

The basis of the nickel-titanium system of alloys is the binary, equiatomic intermetallic compound of Ni-Ti. This intermetallic compound is extraordinary because it has a moderate solubility range for excess nickel or titanium, as well as for most other metallic elements, and it also exhibits ductility comparable to most ordinary alloys. This solubility allows for alloying with many elements to modify both the mechanical properties and the transformation properties of the system.

11

The major physical properties of the basic binary NiTi system and some of the mechanical properties of the alloy in the annealed condition are shown in Table 2.

Note that this is for the equiatomic alloy with an Af value of about 110^oC. Selective work hardening, which can exceed 50% reduction in some cases, and proper heat treatment, can greatly improve the ease with which the martensite is deformed, giving an austenite with much greater strength and creating material that spontaneously moves itself upon heating [34].

Property	Property Value
Melting Temperature (^oC)	1300
Density (gr/cm^3)	6.45
Resistivity (micromho/cm)	
Austenite	100
Martensite	70
Thermal Conductivity (W/m ^oC)	
Austenite	18
Martensite	8.5

Table 2. Major physical properties and some of the mechanical properties of the basic binary NiTi system alloy, from reference [35]

Nevertheless, most of the effort has been focused on incorporating these shape-memory alloy particles or fibers into the liquid tin-silver-copper solder and obtaining a uniform distribution [29, 30]. Because of the non-wetting properties of these two materials, the development of metal coating on micronic particles, with controlled thickness, morphology and adhesion, has been achieved. In literature, electro-less Ni and Cu coatings have been used extensively to promote

the wetting of NiTi, with the solder also providing a diffusion barrier to prevent the formation of intermetallics at the interface between solder and reinforcement. This layer behaves as a sacrificial layer, leading to the absence of the intermetallic formation [31, 32, and 33]. These wetting characteristics have been shown to deteriorate with time and temperature, as the solder is exposed to high homologous temperatures during thermo-cycling. This suggests that the coating approach may not be suitable for microelectronic applications, where multiple reflows are common.

Finally, the CTE of the solder itself could be altered to reduce the thermal stresses that could develop with low-CTE substrates by adjusting the volume fractions of the reinforcements. A composite solder should not be made so strong or rigid that failures will take place primarily in the components [24].

B.   THERMO-MECHANICAL BEHAVIOR OF TIN-SILVER-COPPER SOLDER REINFORCED WITH SHAPE MEMORY ALLOY (SMA)

Solder joints normally experience thermo-mechanical fatigue arising from the thermal expansion mismatch between the coefficient of the ceramic substrate ($6 \times 10^{-6}/{}^{o}C$) and PCB components ($16 \times 10^{-6}/{}^{o}C$) [24]. No improvements in the CTE or replacement of the ceramic substrate have been considered because ceramic is indispensable to meet the rigorous requirements of hermeticity and thermal and electrical conductivity, which are specifically demanded in electronic package technology. Plastic can be investigated for package components (CTE=$30 \times 10^{-6}/{}^{o}C$ but lower stiffness); nevertheless, as the CTE problem increases with the package length, the approach of changing the packaging material would not provide a meaningful solution [35].

When cyclic behavior of a shape-memory alloy is considered, a cycle typically includes loading to a point where a residual strain is present after the load is removed and an apparent deformation has occurred, which is accommodated by detwinning of the martensite phase. Next, the alloy is heated to a temperature at which the material returns to its memorized shape in the

parent austenite phase and maintains that shape upon cooling. This is called a shape-memory effect (SME) cycle [36].

The idea for this is that at low temperatures, SMA fiber/particles are in the soft martensitic state and can, during the raising of the temperature, plastically shear with the solder, which causes the displacement difference between the chip and the PCB. Then, when the working temperature of the chip crosses the martensite-to-austenite transformation temperature, the SMA reverts to the original shape and the transformation strain induces a backstress on the matrix, acting as a reverse eigenstrain and reducing the creep rate at locations where the inelastic strain accumulation is high. Thus, by reducing the inelastic strain in regions near the substrate, the process improves the fatigue life of the solder [5]. This behavior can be seen in Figure 6.
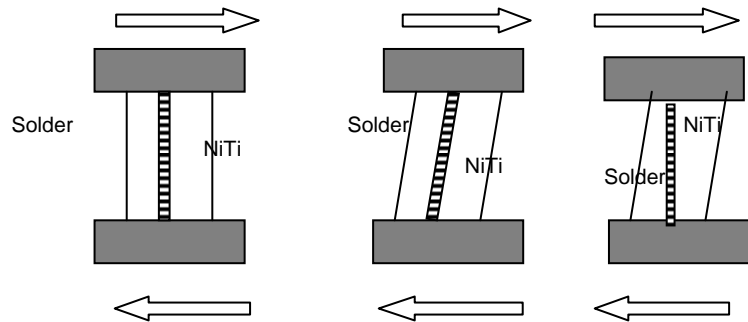
Figure 6.   NiTi Martensite to Austenite Transformation placing solder in reverse shear, after reference [26]

The unique behavior of NiTi is based on a thermo-elastic phase transformation. The high-temperature phase is known as austenite, with an ordered intermetallic crystal structure, and which at particular temperatures or strains transforms into martensite, which has a monoclinic crystal structure. If the parent phase is cooled below M_f (the martensite finishes temperature), the austenite completely transforms into martensite, with the bulk macroscopic shape left intact. However, on the atomic scale, several different martensite variants are

created and twinned to maintain the original bulk shape. There are a total of 24 possible crystallographically-equivalent habit planes of martensite. Once in the martensite form, the material is easily deformable through twinning. Particular variants grow at the expense of others to produce plastic deformation-of-shape change [27]. Figure 7 represent the changes in the crystal form of shape memory alloys which leads to the shape memory effects.
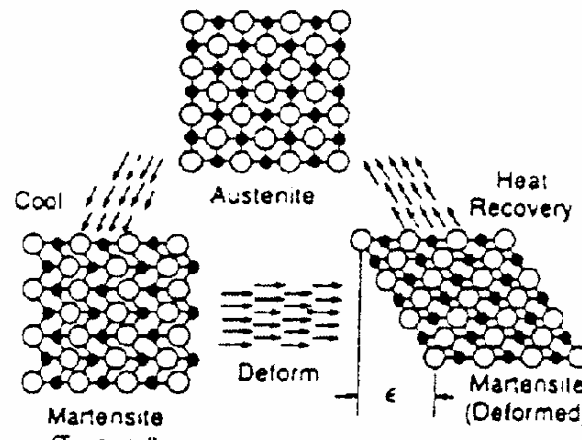
Figure 7.   Crystal reorientation of Shape Memory Alloy during the phase transformations. First the martensitic structure deformed by outer stress into a particular shape, and the crystal structure undergoes parallel registry. Then during the heating the deformed martensite resumes its austenitic form, which finally undergoes twinning as the temperature is lowered, from reference [27]

While most metals deform by slip or dislocation movement, NiTi responds to stress by simply changing the orientation of its crystal structure through the movement of twin boundaries. A NiTi fiber will deform until it consists only of the correspondence variant (crystallographic orientation) that produces maximum strain. However, deformation beyond this will result in classical plastic deformation by slip, which is irrecoverable, and a permanent structure will result [27].

The shape-memory effect occurs when the shape changes through martensitic twin reorientation and then the material is heated above A_f (the

austenite finish temperature) to induce the phase transformation. Since there is only one possible parent phase (austenite) orientation, all martensitic configurations revert to that single defined structure and shape upon heating. This phenomenon causes the fiber to revert completely to the shape before deformation, and thus the material acts like it remembers its original shape. The thermo-elastic martensitic transformation causing the shape recovery is a result of the need of the crystal lattice structure to accommodate itself to the minimum energy state for a given temperature and stress [28].

Figure 8 demonstrates the differential scanning calorimetry (DSC) analysis and free recovery of a NiTi wire. Upon heating, from the equilibrium at -35°C both techniques provide similar A_s (Austenite start temperature), and A_f (Austenite finish temperature) as the monoclinic martensite (B19'-phase) transform completely to the cubic bcc austenite (B2-phase), after a single exothermic peak at 42°C. Upon cooling from the 85°C, at the first peak at 22°C, the wire transform first to a mixture of rhombohedral-martensitic (R-phase) and B19'-phase, prior to the martensitic transformation. The second peak during the cooling, at -35°C, represents the complete transformation of the R-phase to B19'-phase,thus producing a single-phase B19' structure.
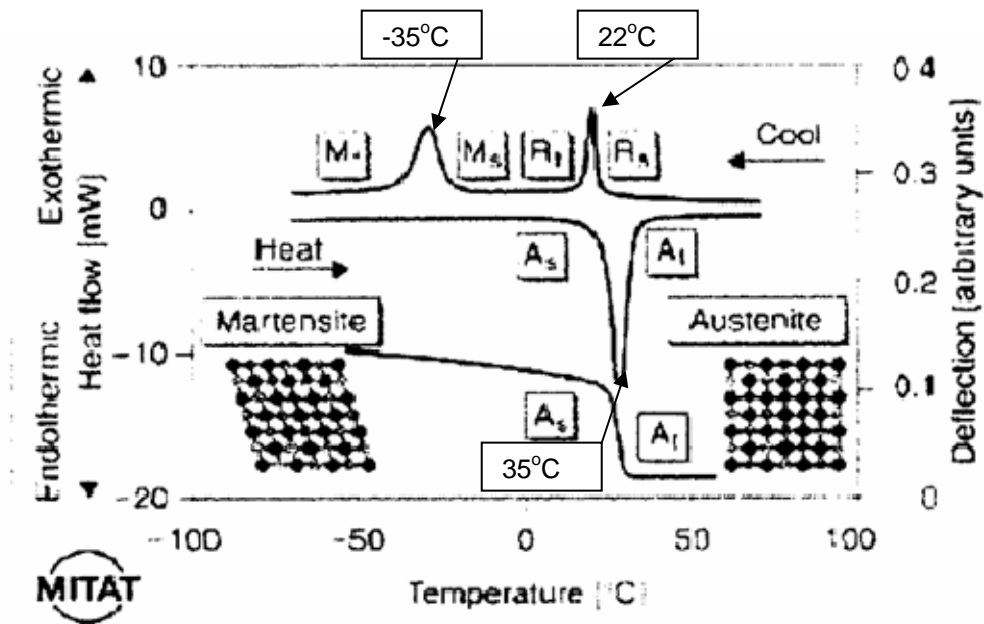
Figure 8.   DSC curves of NiTi wire. Note that upon cooling the wire transforms to R-phase prior to the martensitic transformation. Upon heating, the A_s and A_f temperatures are similar, as the monoclinic martensite transforms to the cubic austenite, after reference [29]

C.   EFFECT OF TIN-SILVER-COPPER SOLDER (REINFORCED WITH SMA) MICROSTRUCTURE ON ITS TMF LIFE

The useful properties of materials are strongly dependent upon their microstructure, which describes the grain structure and the combination of phases present in a material, as well as its defects, morphology and distribution. Generally, for a material of a given chemical composition, the microstructure is not constant and varies greatly, depending on processing and service conditions. In surface-mount assembly, the time-and-temperature-dependent soldering profile affects the microstructure of the solder joints, including the intermetallic layer thickness and the number of intermetallic phases present in the solder joint [40, 53].

Tin-Silver-Copper solder is expected to have better high-temperature performance compared with Sn-Pb solder because of its higher melting

17

temperature and better mechanical properties at room temperature [38]. But, aging studies have shown that the prospective high-temperature application of Sn-Ag-Cu solder needs to be further investigated, as the microstructure of this solder appears unstable at high temperatures [5, 39].

Failure may occur in solder joints just by exposing them to high temperatures. Intermetallic layer growth and crack-and-void formation in these layers are the major sources that induce failure [41, 51]. The intermetallic compounds that are formed at the solder substrate interface continue to grow over time. This growth is a result of a solid-state reaction driven by an energy differential [42]. The solder substrate reaction is exothermic, which means that the intermetallic compounds that are formed have lower energy content than the reacting metals by themselves. Like all reactions, the kinetics of grain coarsening and intermetallic layer growth increase with rising temperatures [37].

The eutectic composition for the Sn-Ag-Cu ternary system occurs at 95.5Sn-3.8Ag-0.7Cu. The microstructure consists of Sn and the intermetallics Ag_3Sn and Cu_6Sn_5 in the form of thin platelets. The solidified microstructure of the ternary eutectic 95.5Sn-3.8Ag-0.7Cu consists of a ß-Sn phase with dendritic globules and inter-dendritic regions with a eutectic dispersion of Ag_3Sn and Cu_6Sn_5 precipitates within a ß-Sn matrix [43, 44].

The most critical soldering parameter that affects the initial microstructure in surface-mount assembly is the cooling rate. One of the desirable properties of potential lead-free solders for SMT applications is having eutectic behavior, where both phases solidify concurrently at a single temperature, rather than over a range of temperatures [45, 46 and 47].

The nature and distribution of the phase mixture of the eutectic composition that is established during solidification is also strongly affected by the cooling rate. Slow cooling, where the solidification reaction proceeds more slowly, results in wider interlamellar spacing. At a sufficiently fast cooling rate, the eutectic structure loses its lamellar character, and a microstructure with fine, uniform dispersion of phases within small eutectic colonies is formed [48].

18

The grain size also varies with the cooling rate. Faster cooling enhances the number of colony nuclei formed, and therefore colony size increases with a slower cooling rate. This microstructural variation, due to cooling rate, can drastically affect the fatigue life of the solder joint [48, 49 and 50].

D. CREEP DEFORMATION KINETICS OF TIN-SILVER-COPPER SOLDER

Since solder joints in electronics packaging experience temperatures greater than one-half their homologous temperatures, it is a reasonable assumption that the same deformation mechanisms observed in creep tests are operative in an electronic package subjected to temperature changes [54]. The low-cycle fatigue-failure response of the solder joints is a creep-fatigue mechanism that involves crack initiation and crack growth, followed by a complete rupture of the solder connection [55].

The steady-state creep deformation kinetics of fine-grained metals and alloys at high homologous temperatures generally exhibit the characteristic behavior given schematically in Figure 9 [56].
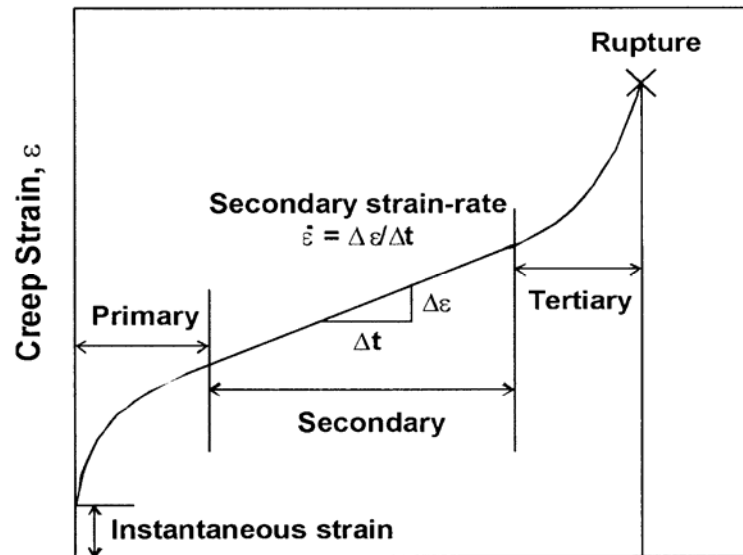
Figure 9.   Creep behavior of metals, from reference [57]

The creep behavior of solder materials in the steady-state creep region is often described by one of the two empirical constitutive equations:

$$\frac{d\gamma}{dt} = A\sigma^n e^{-\frac{Q}{RT}} \quad ....(1)$$

$$\frac{d\gamma}{dt} = A\sinh(\alpha\sigma)^n e^{-\frac{Q}{RT}} \quad ....(2)$$

Where dγ/dt is the steady-state creep rate in shear, A is a constant depending on microstructure, t is the shear stress, n is the stress exponent, Q is the activation energy, R is the gas constant and T is the absolute temperature. Equation (1) is the Dorn equation that works well in the low-stress regime, while equation (2) is the Garofalo-Arrhenius equation that unifies the steady-state creep behavior of solders at the intermediate- and high-stress levels into a single formulation.

Investigation of the deformation behavior for eutectic solders has shown that the deformation in region (II) is controlled by a grain boundary sliding process (super plasticity), whereas the deformation in region (III) should be attributed to dislocation climb and glide. The deformation of region (III) is sometimes called matrix creep [56]. During the developing of the creep, the total plastic shear strain rate finally controlled only from the matrix creep as the phase coarsening of the solder reduce the grain boundary areas and make difficult the grain boundary sliding process. But the region (III) is more severe for the solder and is this which finally induced the failure.

For the tin–silver-copper eutectic solder in the as-reflowed state, the microstructure, which consists of secondary dendrites of β-Sn interspersed with a highly refined divorced eutectic structure of fine particles of Ag_3Sn and Cu_6Sn_5 in a β-matrix, allows for supersaturation of the β-Sn. The overall deformation of the

composite microstructure (divorced eutectic and primary β-Sn) is controlled by the behavior of the eutectic, which deforms via glide-climb at low stresses and by particle-limited climb at high stresses [57].

In 95.5Sn-4.0Ag-0.5Cu alloy, Ag_3Sn elongated precipitates were found under SEM by Li Xiao et al [59]. With the help of TEM analysis, tiny dispersed Cu_6Sn_5 precipitates with size around 50-nm were found in the Sn matrix. Therefore, the strength behavior of this alloy should be enhanced. It already has better high-temperature creep resistance than other eutectics solders [56].

THIS PAGE INTENTIONALLY LEFT BLANK

III.   EXPERIMENTAL PROCEDURE

In order to demonstrate the effects of the shape-memory alloys when used as reinforcements in microelectronic solder joints, six different types of solders were created and exposed to aggressive thermo-mechanical cycling conditions similar to those of the real world. Comparison of the thermo-mechanical responses of these samples can yield direct evaluation of the role of the reinforcements. As a result, TMC studies were conducted on monolithic 95.5Sn-3.8Ag-0.7Cu solder, NiTi rod-fiber-reinforced solder, NiTi flat-fiber-reinforced solder, Cu rod-fiber-reinforced solder, Cu flat-fiber-reinforced solder. Also, an attempt to fabricate NiTi particulate-reinforced eutectic solder, using the sintering method by mixing NiTi and 95.5Sn-3.8Ag-0.7Cu powders is presented. The procedures followed for preparation and testing of the samples are discussed below:

A.   SOLDER FABRICATION
1.   Monolithic Tin-Silver-Copper

For this kind of solder, sheets of 1-mm thickness cold-rolled 96.5Sn-3.8Ag-0.7Cu were used, from which disks with 3-mm diameter and 1-mm thickness was created. The surface of the disks was sanded and cleared using acetone to remove the oxidate film, and then joined together using an adipic acid-based flux with polyethylene glycol and polypropylene glycol as the thixotropic agent and solvent. This flux uses a low-reflow temperature and is self-cleaning.

In order to produce this flux, 20 grams of polyethylene glycol (PEG, Aldrich #20,243-6)--a white waxy solid, 15 grams of adipic acid (Aldrich # A2635-7)--a white solid powder, and 50 grams of polypropylene glycol (PPG, Aldrich #20, 235-5)--a transparent glycerin-like liquid were placed and mixed together with a stir-pak laboratory mixer using an impeller type blade, at a speed of 50 to 100 RPM. The mixture began to smoke when heated to 150$^{\mathrm{o}}$C, and when it reached 200$^{\mathrm{o}}$C the speed of stirring was increased to 200-300 RPM until the

23

mixture took a single-phase appearance with no particulates. After this, the mixture air cooled to 120$^{\text{o}}$C while stirring speed was maintained, and it was finally quenched rapidly in a water bath in order to break down the adipic acid precipitates into fine 25-micron particles. Finally, the stirring was continued until a solution temperature of 30$^{\text{O}}$C was reached, and the resultant flux was sealed in a bottle at room temperature.

2. NiTi Rod-Fiber Reinforced Solder

The commercially available NiTi wire with 1-mm diameter was purchased from Dynalloy Corporation, Costa Mesa, CA and contains approximately 50.6% Ni, having an austenite start temperature A_s of ~40$^{\text{o}}$C.

Before the fabrication of the single-fiber composite, the wire first annealed at 550$^{\text{o}}$C for 30 minutes, followed by air quenching. The transformation point of the NiTi after the heat treatment was measured using the differential scanning calorimeter (DSC). DSC testing is a thermal method that measures the change in heat flow that is associated with the martensitic and austenitic phase transformations, through a controlled cooling-heating cycle. It shows that the austenite transformation temperature is at 42$^{\text{o}}$C.

Also, for the solder, reinforced with NiTi fiber and NiTi particles, it was known that during the thermo-cycling these reinforcements would act as an adaptive or smart alloy, and not as a passive one. As the temperature during cooling reached -15$^{\text{o}}$C, the fiber would totally recover to its original Martensitic phase, with all the beneficial effects that this transformation would have in the accumulation of inelastic strain to the solder.

Next, the wire was ground with emery paper to remove the oxide film from the surface of the rod shape wire. As the NiTi alloy is highly reactive with the atmosphere, it tends to create a very thin film known to have amorphous, homogeneous and non-porous composition.

This oxide layer is composed essentially of TiO_2 with some impurities on the surface due to environmental handling. A NiTi surface is mostly composed of

titanium oxides and, to a lesser extent, nickel oxides, while nickel-titanium constitutes the inner layer. Nickel may initially dissolve more easily than titanium because its oxide is not so stable. After that, the surface contains more titanium oxide. The good corrosion resistance of NiTi is thought to be mainly due to its ability to form this stable Ti oxide layer.

But this oxide layer also creates problems for the bonding or the wettability of the NiTi wire with other alloys. So, in order to improve the wetting ability of the wire with the tin-silver-copper solders a hydrofluoric-acid-based liquid flux, IndalloyFlux #2 (Indium Corp. of America) has been employed to eradicate the oxides on NiTi surfaces.

Before the wire is placed in the graphite mold, it is heated in the flux at 150°C for 3 minutes. The flux reacts with the oxide layer of the base alloy, and removes or loosens it from the alloy's surface. The molten flux then forms a protective blanket that prevents re-formation of the oxide film until molten solder displaces the flux and reacts with the base metal to form an intermetallic bond. So, the effectiveness of a flux is a combination of desirable properties such as: a melting point slightly below the soldering temperature, ability to remove oxides, ability to protect metal surfaces from further oxidation and electrical nonconductivity after soldering.

In order to achieve the best wetting between NiTi wires and solder, different approaches were developed during the preparation of the composite solder. According to Table 3, different temperatures for the heat-treating of the wire, and different times in contact with the solder, result in different quality where the wetting between wire and solder is concerned. Increasing the temperature where flux and wire are heated, before the casting of solder, develops a very good wetting.

But this is not always the rule. Heating the SMA fiber with the IndalloyFlux #2 for an extensive time period (for example, 30 minutes), gives rise to the diffusion phenomenon of the H^+ (from the HCl or HF contained in the flux) inside

the fiber, which embrittles the alloy, deteriorates its composition, and finally reduces or removes the shape-memory properties of the alloy.

Flux Temp. (°C)	Time (min)	Solder Temp. (°C)	Time (min)	Wetting
25	1	260	10	poor
50	1	260	5	poor
70	3	260	15	good
100	1	260	15	Very good
	3	260	15	Very good
150	3	260	15	Very good

Table 3. NiTi Wetting procedure data with flux II

Finally, the composite solder was fabricated by casting tin-silver-copper alloy around the NiTi fiber at 240°C for 20 minutes. After the solidification in order to make the NiTi fiber to be in Martensite phase, the solder were quenched into cold acetone solution at -20°C and then pieces of 3-mm length were cut from this pre-made reinforced solder using a diamond-edge saw.

3.   NiTi Flat-Fiber-Reinforced Solder

The procedure for the fabrication of this ribbon-like reinforced-fiber solder was the same as for the NiTi-rod fiber, except for the fact that the wires were first annealed at 600°C for 2 hours in order to recover the plastic strain before they were placed in the liquid solder matrix, and then rolled in flat strips with thickness 200-μm.

4.   NiTi Particle-Reinforced Solder

For the production of this kind of solder, NiTi powder with 10 to 20-μm-sized particulates need to be created.

So for the powder production, the commercial NiTi wires of 1 mm thickness from Dynalloy Corporation were used, first hydrogen-embrittled and then carefully ground to powders less than 20-μm by mechanical grinding in a mortar and pestle. Before the hydrogen embrittlement of the wires, their surfaces were carefully ground with 400-grid silicon-carbide sandpaper in order to remove the oxide layer. After this, they were annealed at 600°C for 2 hours and then rolled into flat strips with 200-μm thickness. Then, an electrochemical cell was produced in order to cathodically charge the NiTi with H, using a solution of one normal of sulfuric acid (H_2SO_4) and 0.2 grams per liter of Thiourea (Aldrich chemical T33553-500g), with a 0.5-mm-diameter platinum wire in coil shape as anode and the NiTi wire as cathode. A Hewlett Packard power supply was used with 0-10 Volts and 35 Ma/cm^2 ranges to deliver a current density of 35 mA/cm^2 so the required H_2 would diffuse into NiTi.

The experimental setup for the above procedure can be shown in Figure 10.
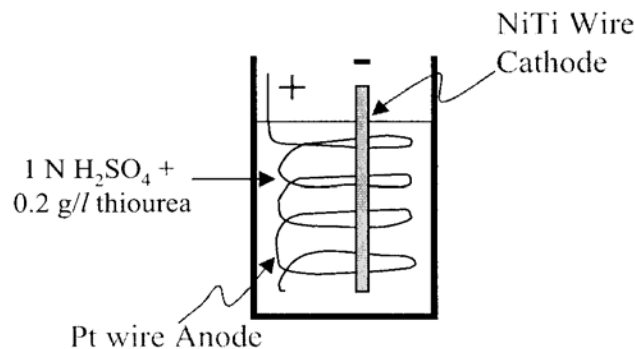

Figure 10.   Hydrogen embrittlement setup, from reference [26]

After the wires embrittled for 15-20 hours in the above solution, they were cleaned with water to remove the residual acid solution and then air-dried. Finally, the embrittled NiTi strip was ground down to an average size of powder of 20-μm using mechanical grinding. In order to recover the amount of cold work which delivered to the NiTi particles during grinding, they annealed at 550°C for 3 hours.

Also, DSC analysis of the cold-worked powder with hydrogen impurity did not show any shape-memory effect. However, a de-hydrogenation process, at 550°C in vacuum for half an hour, recovered the shape-memory effect of the NiTi powder. This recovered NiTi powder, as Figure 11 shows, exhibits lower A_s and A_f transformation points and an increase of the M_s transformation point, the starting point of the austenite-to-rhombohedral-martensitic phase.
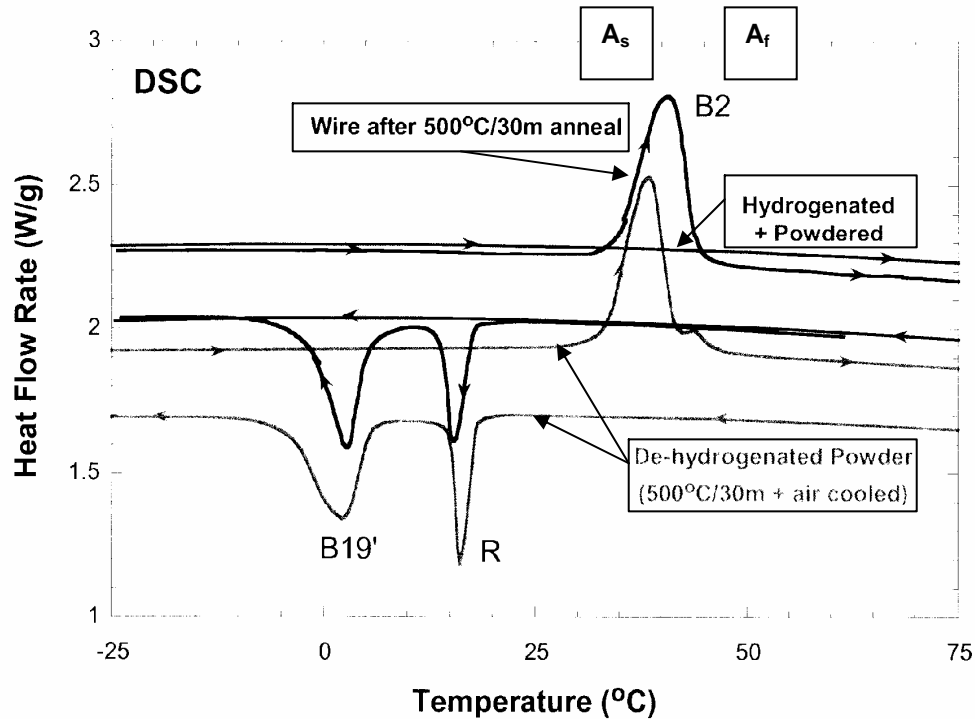

Figure 11.   Effects of Hydrogen embrittlement on NiTi

For the preparation of this kind of composite solder, eutectic 95.5Sn-3.8Ag-0.7Cu powder with a size range of 40-50 μm was mechanically mixed (at 50 rpm for 60 minutes) with NiTi particles of size less than 38 μm to create a composite powder of 10% NiTi particles. Then, the mixed powder was cold-compacted at 25 MPa for 20 minutes and sintered at 210°C for 12 hours.

The solder thus produced was mechanically polished, following the same procedure as described later for the other solders, and the microstructure was evaluated by optical microscopy.

Figures 12 and 13 show the solder microstructure at 290× and 1500×, respectively. The eutectic solder with the Ag_3Sn and Cu_6Sn_5 precipitants in the β-Sn matrix shows a good dispersion of the NiTi particles. The extrusion of the solder would induce plastic deformation, which would probably break the oxide layers and eliminate any holes between the powder particles.
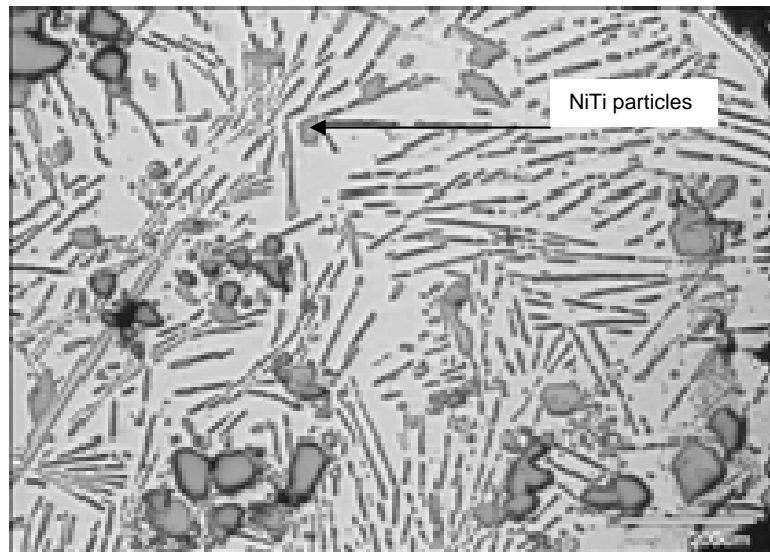

Figure 12.   290× Optical microscopy picture of the NiTi reinforced solder
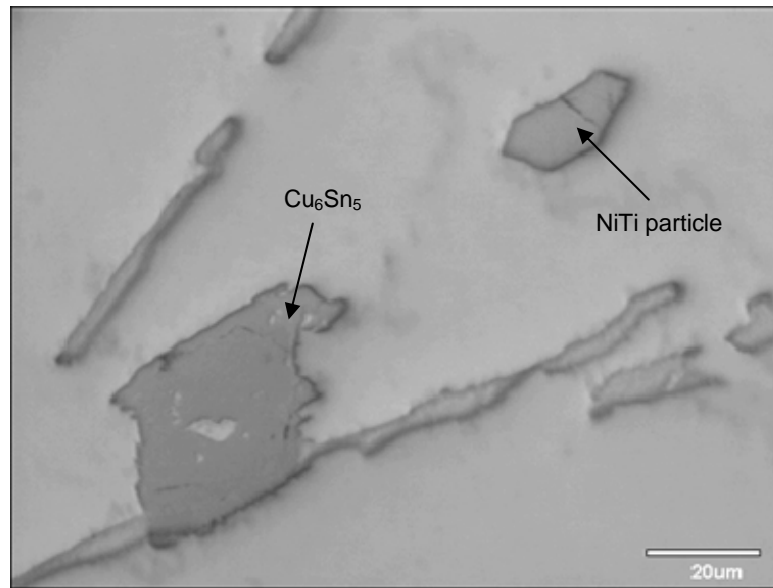
Figure 13.   1500× Optical microscopy picture of the NiTi reinforced solder

5.   Cu Rod and Flat-Fiber Reinforced Solder

Solders similar to those of the NiTi reinforcements were created using Cu fiber as a passive reinforcement in order to determine, by comparison with the monolithic, the stress-strain response of the solder. Information and details on the preparation and fabrication of these solders and samples can be found in Reuse Ronaldo's 2005 Naval Postgraduate School thesis.

However, analysis and comparison of the thermo-mechanical behavior of these Cu-reinforced samples are presented later in the results and discussion chapter.

B.   SAMPLES PREPARATION

1.   Cylindrical SJS Joints

For comparison of the various materials, cylindrical single-joint samples were created using 99.9% pure copper rods with a length of 19-mm and a diameter of 5.9-mm. The rod ends had a recessed cup 3.175-mm in diameter,

with a depth of 0.38-mm, placed on one rod end. The sample geometry is schematically depicted in Figure 14.
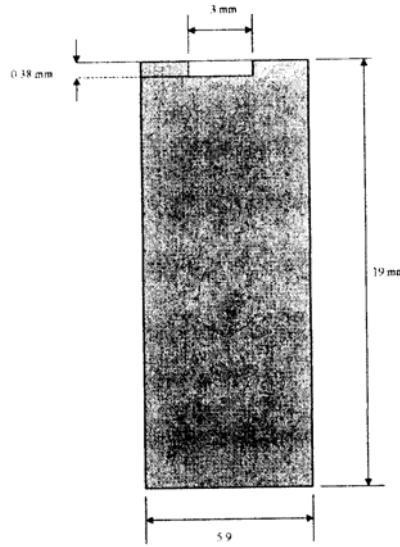
Figure 14.   Cylindrical (Recessed Cup) type Cu rod, from reference [26]

These pure-shear specimens have a small joint thickness compared to the area of the solder, thereby minimizing the tensile stresses associated with bending moments.

A thin film of aluminum was deposited on this surface end, using a high-vacuum Vapor Deposition Chamber. The PVD chamber used two tungsten-wire baskets with cleaned pieces of pure aluminum where the vacuum was drawn down to 5×10^{-8} torr and the copper rods heated to $155^{\circ}C$. Then, current was applied to the tungsten baskets until 25 Ampere per minute of current was achieved, and the evaporation of the aluminum began. The PVD chamber can be seen in Figure 15.
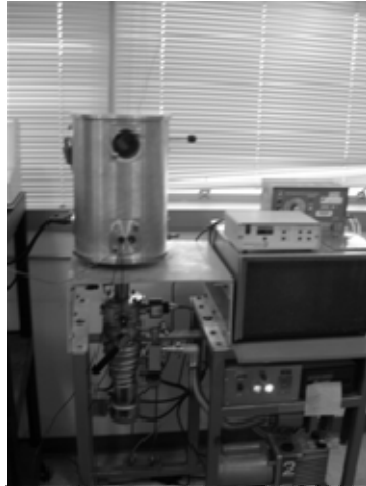
Figure 15.   PVD chamber with attached Diffusion pump

Silicon carbide 1000-grid was used first, and 4000-grid later, to remove the aluminum film from the inside of the recessed cup end. The rest of the upper perimeter of the rod end was protected from the thin film--as it acts as a barrier for the reflow solder due to the bad wetting between copper and aluminum--thus providing a regular cylindrical shape joint.

Next, the area of the recessed cup was rinsed with distilled water followed by methanol, and then dried. A small dab of flux was applied to the recessed cup, and solder disks of the appropriate type (6 monolithic disks, or one NiTi fiber and NiTi particulates in the case of reinforced solder) with 0.7-mm height and 3-mm diameter were placed between the two copper rods.

The final shape for the monolithic solder joint is shown in Figure 16.

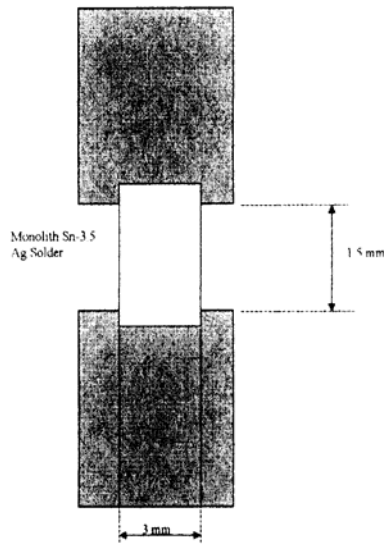Figure 16.   Nominal Recessed Cup Monolith sample size/geometry, from reference [26]

The copper rods, with the solder in contact, were placed in a removable aluminum crucible, inside the 500W 120VAC radiant ceramic furnace, as Figure 17 show, with the upper rod fixed and the lower rod free to move in the vertical direction. The height and the width of the solder could then be adjusted using the anvil of a micrometer. The micrometer was controlled with an electric motor, wired to a DC power supply and providing positive control of the dimensions of the joint. As the furnace initially heated to $290^{o}C$, the solder reached $200^{o}C$ in about 30 minutes; the temperature of the furnace was then reduced to $250^{o}C$ in order to maintain a reflow temperature of the solder at $240^{o}C$ for 10 minutes. During this reflow period, the joint height was adjusted using the electric motor-micrometer to 1.3-mm. These adjustments also helped to remove the air trapped inside the solder and ensure good contact of the fiber (in the case of reinforced solder) with the two copper rods. After the heating phase, a fan was used to cool the joint at a rate of $10^{o}C/sec$.
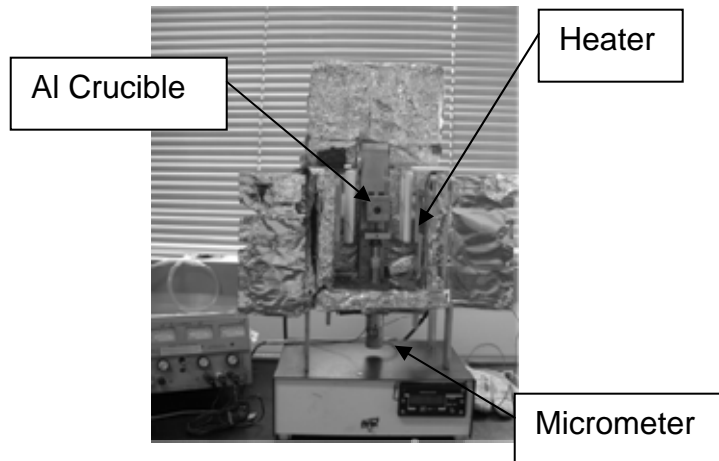
Figure 17.   Heater Ceramic furnace with micrometer

Macrographs of samples with cylindrical SJS joints (produced by the above method) of the monolithic, the single NiTi fiber composite, the single NiTi tape composite and the Cu-reinforced solders are shown in Figures 18-22.
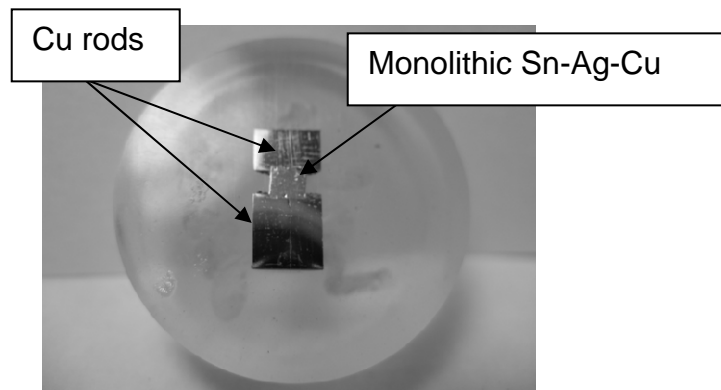
Figure 18.   Macrograph of monolithic cylindrical SJS sample
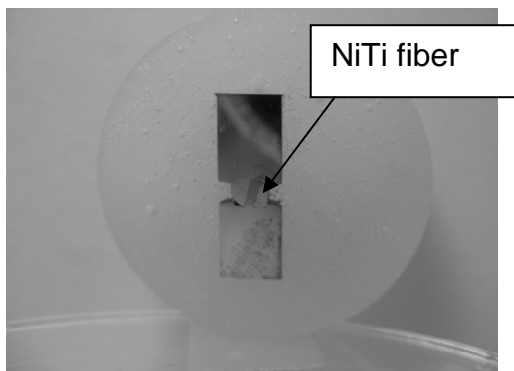
Figure 19.   Macrograph of NiTi fiber cylindrical SJS sample
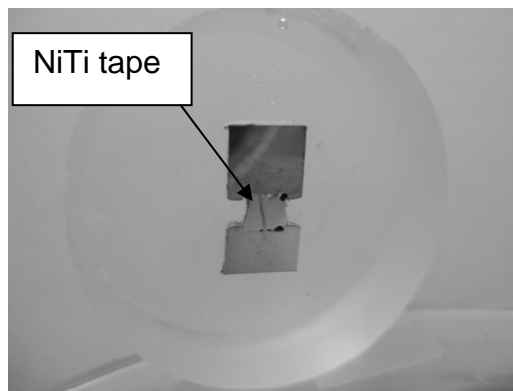
Figure 20. Macrograph of NiTi tape cylindrical SJS sample
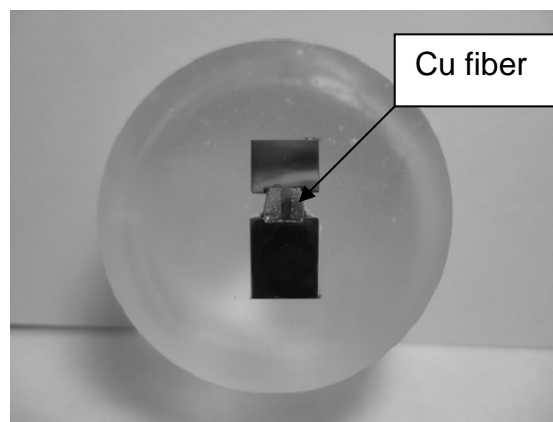
Figure 21. Macrograph of Cu fiber cylindrical SJS sample
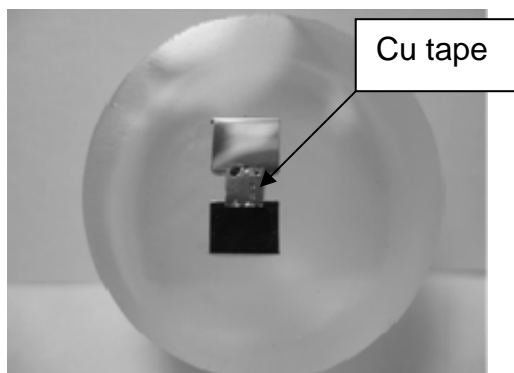
Figure 22. Macrograph of Cu tape cylindrical SJS sample

This method proved to be very reliable compared with other techniques that have been used in the past for the formation of the SJS, especially for reinforced solders with fiber, where the contact of the fiber edges with the copper rod interface is critical to the reliability of the solder. Also, the visible contact of the solder during the whole reflow procedure offers many opportunities for controlling the reflow temperature and the characteristics of the solder.

C.   BIMETALLIC LOAD FRAME FOR TESTING

The thermo-mechanical fatigue behavior of solder joints in shear was recorded using an experimental apparatus, which consisted of a loading frame and a temperature-cycling chamber. This fixture--which was used to stress the samples--had been designed and used by previous researchers, as in References [54] and [25].

After the specimen was inserted and clamped in the bimetallic frame, the fatigue tests were performed by ramping them in triangular waveform between the temperature extremes of -15 and 120°C. This triangular waveform, as the Figure 23 shows, seems to be a simplification of the actual temperature-time profiles that the solder experiences during the operation of an electronic device. The avoidance of dwells at the maximum and the minimum temperatures resulted in a slow transfer of elastic energy from the loading frame to plasticity in the solder, and a lowering of the number of cycles for fatigue life.
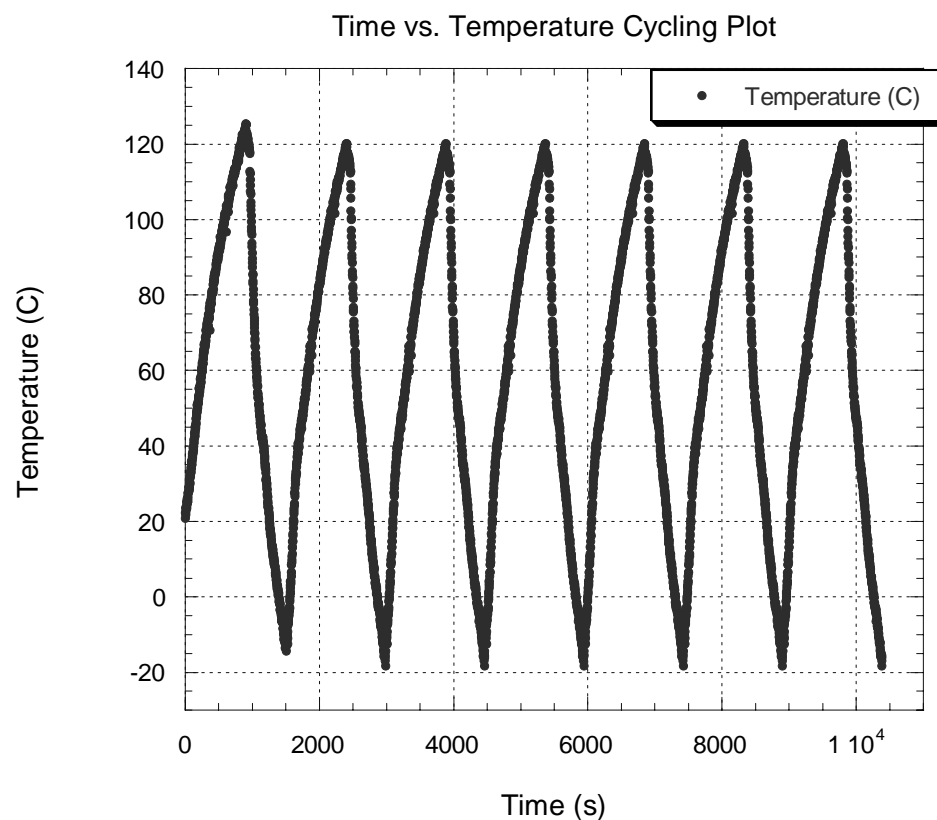
Figure 23.   Temperature vs. Time fluctuation during the testing cycling

The cycling was accomplished in a chamber furnace maintained at 245°C by a closed-loop controller and with a direct-spray discharge of liquid nitrogen, mounted to the underside of the furnace (using an appropriate nozzle), onto the sample. A pneumatic ram controlled the movement of the sample from the cooler to the furnace. A timer and two solenoid valves were used to send low-pressure air to the top and bottom parts of the ram in order to move it up and down. The timer was programmed to cycle the solenoid valves and control the thermo-dynamic profile. Every cycle consisted of 15 minutes inside the furnace and 10 minutes outside. The liquid nitrogen valves opened after the first 9 minutes of cooling at room temperature.

A schematic representation of the bimetallic loading frame with specimen inserted, and the thermal cycling apparatus that was used, can be seen in Figure 24 and Figure 25 , respectively.
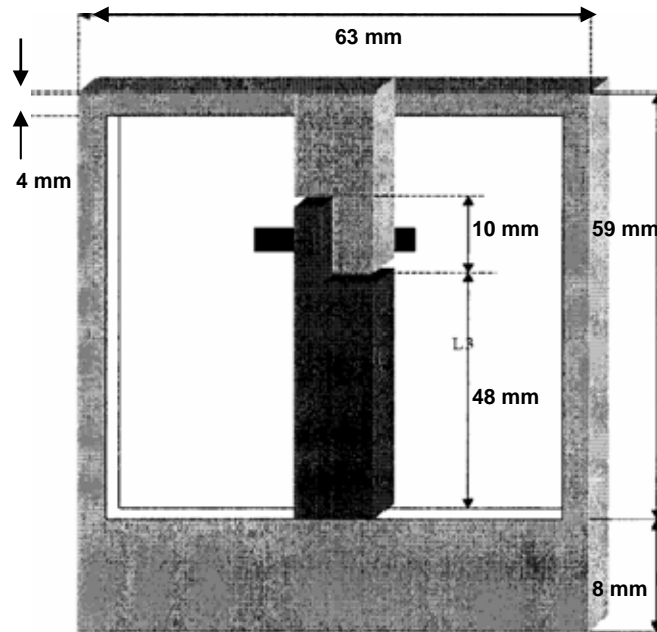
Figure 24.   Bimetallic frame with specimen inserted, after reference [26]

This bimetallic frame consists of one leg made by Invar, with a coefficient of thermal expansion (CTE) $\alpha=7.20e^{-7}$/K; the rest of the frame is made of an aluminum alloy with a (CTE) $\alpha=2.28e^{-5}$/K. This significant difference in the order of magnitude of the CTE between the two parts of the frame induces a shear displacement in the solder during the heating and cooling of the experimental apparatus according to the equation $\delta=\Delta\alpha\cdot\Delta T\cdot L$, where the temperature difference ΔT was measured by two thermocouples attached to the specimen. The design of the frame was such as to ignore normal components of stress due

to bending moments on the solder joint, and the frame had a nominal shear-strain range of about 0.03 in the experimental temperature range. Also, according to [54] it was assumed that the effects of bending moments during the plastic deformation of the solder would not detract from the analysis. The dimensions of the frame were chosen so that the output signals of the strain gages were maximized and at the same time were not too compliant compared with the solder. However, as the sample resisted the shear from the thermal mismatch, it caused deflection in the upper beam of the frame.
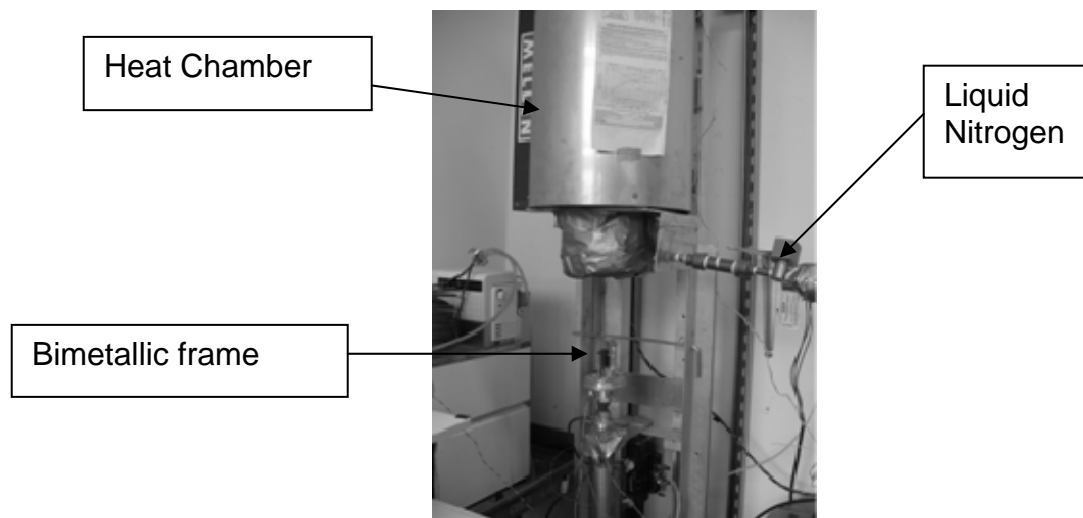
Figure 25.   Thermal cycling apparatus

The load and the mechanical (stress-induced) strain in the system during the thermo-cycling were collected by four Wheatstone strain gages. A 10VDC power supply provided the excitation voltage, while a signal conditioner amplified the output 50X. The resistant self-temperature-compensated strain gage bridges were placed in pairs--two on the top of the top member of the frame and two at the bottom--and carefully selected in order to satisfy the designations of Micro-Measurements' self-temperature-compensated strain gages.

According to these designations, once an installed strain gage is connected to a strain indicator and the instrument is balanced, a subsequent

change in the temperature of the gage will normally produce a resistance change in the gage. This temperature-induced resistance change is independent of and unrelated to the mechanical strain in the test object to which the strain gage is bonded. It is purely due to temperature change, and is thus called the thermal output of the gage. In fact, when measuring strains at temperatures remote from room temperature or the initial balance temperature of the gage circuit, the error due to thermal output, if not controlled, can be much greater than the magnitude of the strain to be measured.

So, with thermal output expressed in strain units, corrections are made by simply subtracting (algebraically, with sign) the thermal output from the indicated strain. The first step in the correction procedure is to refer to the graph that included on the Technical Data Sheet which accompanying each package of Micro-Measurements self-tempe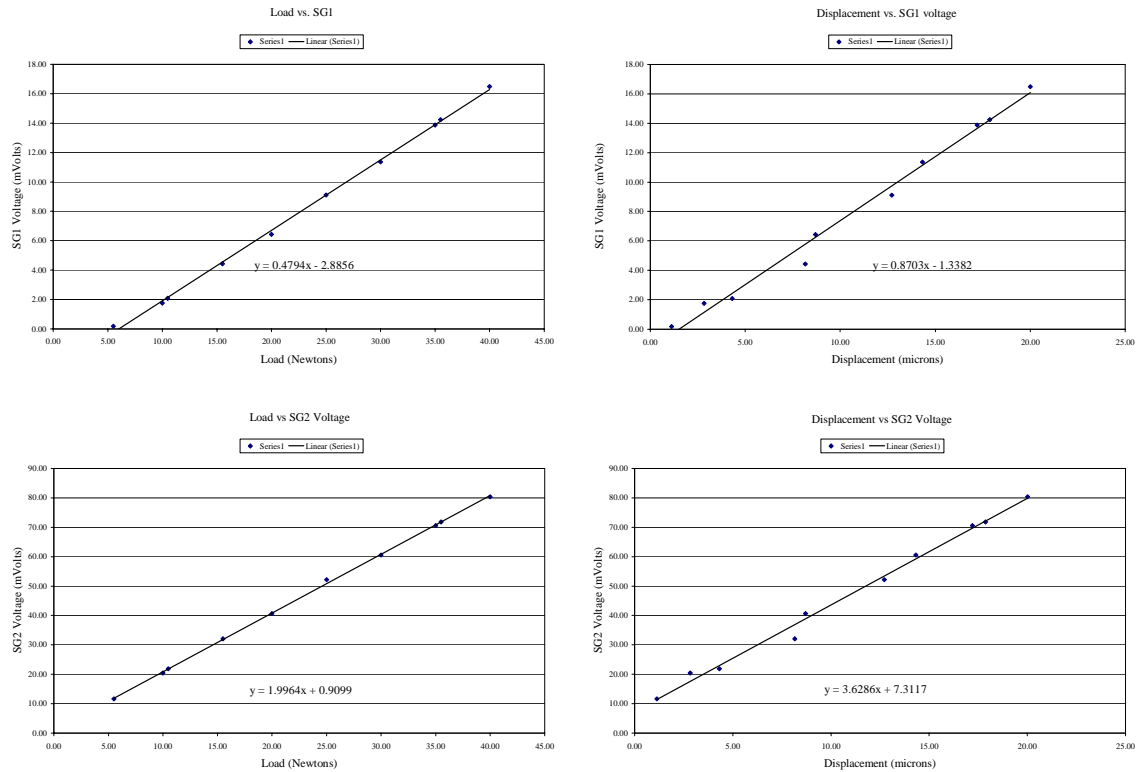rature-compensated strain gages, and read the thermal output corresponding to the test temperature. Then, assuming that the strain indicator is balanced for zero strain at room temperature, subtract the thermal output given on the graph from the strain measurements at the test temperature, carrying all signs. This artificial signal was determined by measuring the strain gage output of the frame with no specimen mounted. This was done for each of the temperature-cycle profiles.

Calibration of the loading frame was carried out to experimentally determine its mechanical properties, that is, the frame stiffness and the effective thermally induced displacement over the specimen grips. The calibration procedure consisted of determining the linear relationship between Voltage/Load (mVolts/Newtons) and Voltage/Displacement (mVolts/mm) and, from these two, extrapolating the final relationship with Load/Displacement (Newtons/mm), which gives the stiffness of the frame.

The frame was placed in an MTS load unit, with a known displacement and load imposed to obtain the values for the mm/V and N/V. The results of the linear plots can be seen in Figure 26.

Load vs. SG1	Displacement vs. SG1 voltage
y = 0.4794x - 2.8856	y = 0.8703x - 1.3382

Load vs SG2 Voltage	Displacement vs SG2 Voltage
y = 1.9964x + 0.9099	y = 3.6286x + 7.3117

STRAIN GAGE	VOLTAGE vs. LOAD	VOLTAGE vs. DISPLACEMENT
SG 1	0.0056497 V/N	9.0992 V/mm
SG 2	0.0059630 V/N	9.6339 V/mm

Figure 26.   Calibration plots of the frame and results for the linear constants for Voltage/Load (mVolts/Newtons) and Voltage/Displacement (mVolts/mm)

Based on observed mechanical response and theoretical considerations, empirical and semi-empirical equations were used to describe the behavior of the

solder during deformation. In such a manner, the mechanical state of the system after an increment in temperature ΔT and time Δt can be calculated.

During the thermo-cycling of the frame as an assembly, its shear displacement due to CTE difference is equal to the sum of the total displacement of the frame and the displacement of the solder deflection:

$$d_{thermal} = d_{solder} + d_{beam} \Rightarrow L\Delta\alpha(T - T_0) = h(\gamma_{el} + \gamma_{pl}) + \frac{\tau A}{K}$$

Where L is the distance between the solder joint and the neutral point, h is the thickness of the solder joint, A is the cross-sectional area and Δα is the difference in CTE. The displacement from the thermal mismatch is accommodated by a combination of elastic and plastic shear strains of the solder, γ_{el} and γ_{p}, respectively.

If the solder joint and package assembly are instantaneously subjected to a small increment in temperature ΔT, the assembly components will change dimensions according to their respective coefficients of thermal expansion, thus creating a stress-and-strain state in the system. The strain must be absorbed elastically in the solder γ_{el}, or in the surrounding assembly as described by the term $\frac{\tau A}{K}$, with no plastic strain. Also, the change in elastic displacement is given by $\frac{\Delta\tau}{G(T)} * t_{JOINT}$. The resultant instantaneous stress change is given by:

$$\Delta\tau = \frac{L\Delta\alpha\Delta T}{A} \left[\frac{1}{\left(\frac{1}{K} + \frac{h}{AG(T)}\right)} \right]$$

This yields the equation for the change in shear at the solder joint:

$$\Delta\tau = \frac{kCV_{SG}}{A_{JOINT}} \tag{1}$$

For the change in shear strain during the test ($\Delta\gamma_{TEST}$), an addition of the change in elastic ($\Delta\gamma_{ELASTIC}$) and plastic shear strain ($\Delta\gamma_{PLASTIC}$) gives the following equation:

$$\Delta\gamma_{TEST} = \Delta\gamma_{ELASTIC} + \Delta\gamma_{PLASTIC} = \frac{\Delta\tau}{G(T)} + \Delta\gamma_{PLASTIC} \Rightarrow$$

$$\Delta\gamma_{PLASTIC} = \Delta\gamma_{TEST} - \frac{\Delta\tau}{G(T)}$$

(2)

The calculation of the shear stress and the total plastic shear strain in the solder joint can be accomplished by the equations **(1)** and **(2).** Using the constant values for Voltage vs. Displacement and Voltage vs. Load, the average shear stress and the inelastic shear strain can be iterated over each thermocycle, with a step time of 2 sec.

THIS PAGE INTENTIONALLY LEFT BLANK

IV. RESULTS AND DISCUSSION

A. MICROSTRUCTURAL DETERMINATION

All the samples were air cooled after the reflow, and cut in half sections using a diamond saw. They were then fixed in epoxy bases in order to be polished, following a mechanical polishing schedule, as follows. First, as the eutectic solder is very soft, sand it sequentially with 1000-, 2400- and 4000-grid silicon sand paper. Next, use a sonic bath to create a smooth surface without scratches. Then, employ a 1-µm polishing cloth with Al_2O_3 solution added. As the final step, a 0.05-µm cloth with colloidal SiO_2 added gives a very shiny view of the solder.

The figures below illustrate the composition of the ternary, eutectic, cylindrical solder SnAgCu with or without reinforcement; the appearance and the composition of the intermetallic particles inside the solder; and the characteristics of the intermetallic layers between solder and reinforcements.

Figures 29(a) and 30 show the microstructure of the monolithic solder, which consists primarily of β-Sn grains surrounded by a divorced eutectic of fine Ag_3Sn and some bigger Cu_6Sn_5 intermetallic particles in Sn. In Figure 29(b) can be seen the interfacial Cu_6Sn_5 layer between the Cu rod and the solder, which consists of a brittle substrate.
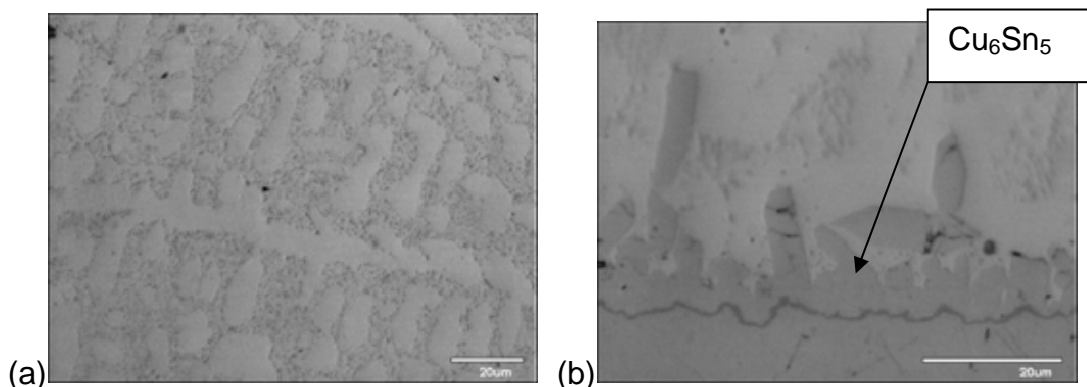

Figure 27.   (a) Microstructure of SJS joint of a monolithic solder (1500× optical magnification) and (b) interfacial Cu_6Sn_5 layer between the Cu rod and the solder

This solder was solidified at a low cooling rate, at room temperature, and for this reason contains a smaller number of larger Ag_3Sn precipitates compared with a solder in the flip-chip joint, where the higher cooling rate yields a high number of precipitates, but with smaller dimensions.

At the same volume fraction of precipitates, a higher number of smaller particles act as a more potent obstacle to the movement of dislocations than does a smaller number of larger particles, which results in a more creep-resistant mechanism.
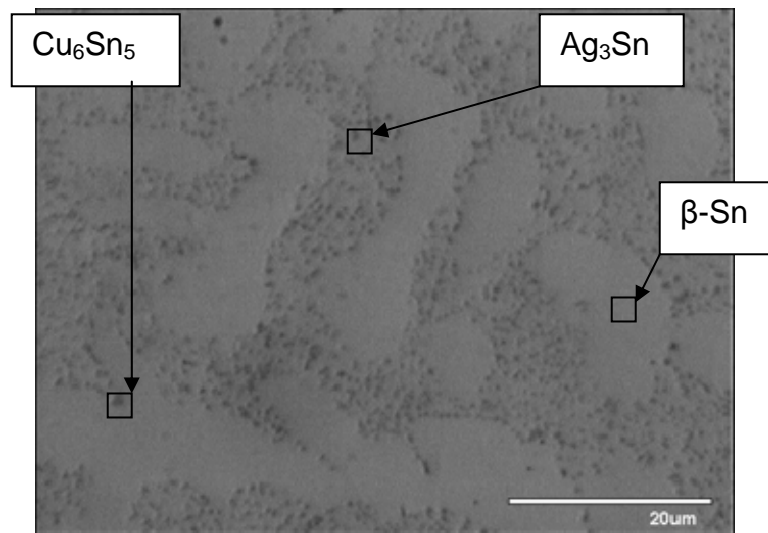
Figure 28.   3000× optical magnification of monolithic solder where the intermetallics precipitates Cu_6Sn_5, Ag_3Sn and Primary β-Sn shows better

Also, there is another important role that these intermetallics play during the deformation of the eutectic solder. Specifically, the stability of the whole microstructure in these lead-free solder joints is chiefly determined by the resistance to coarsening of the dispersed phase. When the moving boundaries attach to the intermetallic particles, the particles will exert a pulling force on the boundary restricting their motion. Furthermore, the stabilization of a fine-grain size during heating at high temperatures also requires the stability of small

particles. For this lead-free solder, the Ag_3Sn phase is the major dispersed phase, whose melting temperature is 480°C. This suggests that it has a relatively higher recrystallization temperature.

In view of the above, and with the fact that the SnAgCu solder has limited solubility of Ag in Sn, which makes it more resistant to coarsening, it is obvious that the shear strength of the lead-free solder is greater than that of the lead solder, where the phenomenon of microstructural coarsening is more pronounced.
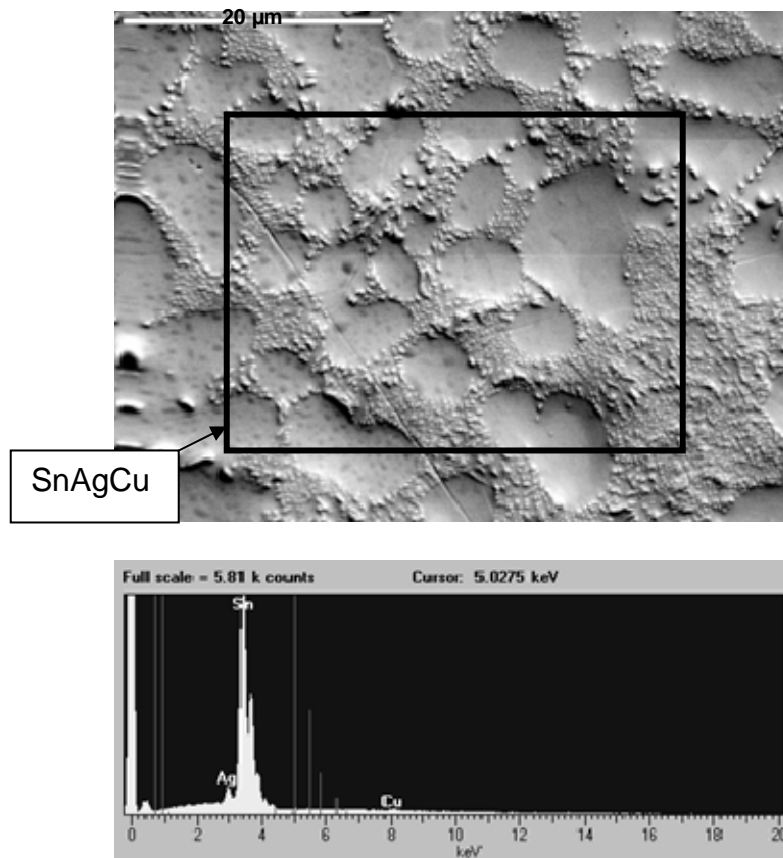
Figure 29.   The microstructure of the cross-sectioned SnAgCu solder, using SE microscopy, and the composition results from all the solder of the figure using EDS analysis

.

As Figure 29 shows the composition of the solder which used is 93.91Sn-4.90Ag-1.19Cu. This results from the EDS analysis of all the solder region of Figure 29.

As free-growing crystals, each of the solid phases involved in the solidification reaction of the eutectic solder has a distinct morphology, making them easy to identify when observed in cross section. The tin solid-solution phase in the solidification of microstructures is generally manifested as non-faceted dendrites with no strong crystallographic orientation. The Cu_6Sn_5 phase generally forms as an acicular or hexagonal-shaped phase, while the Ag_3Sn phase generally forms in platelike morphologies.

The Ag_3Sn phases were identified for the region that Figure 30 shows both by their morphology and by the absence of a copper peak in the EDS spectrum.
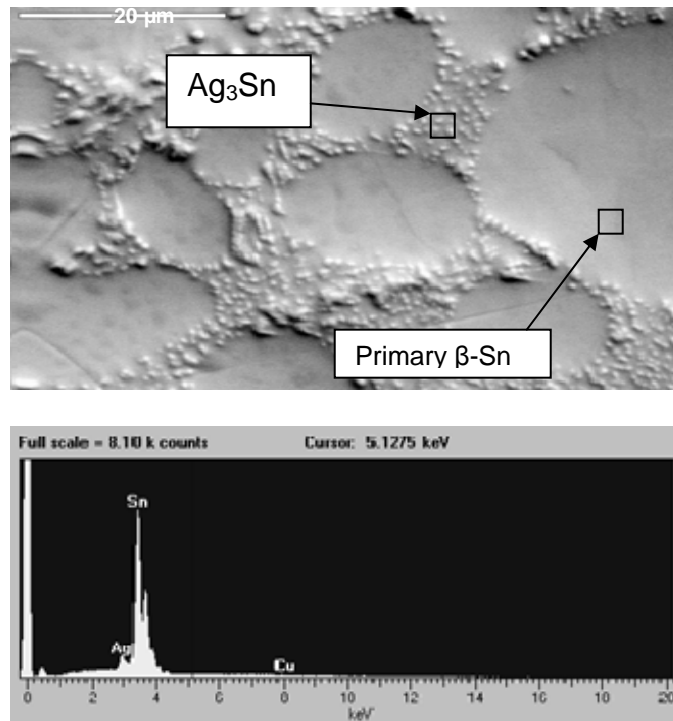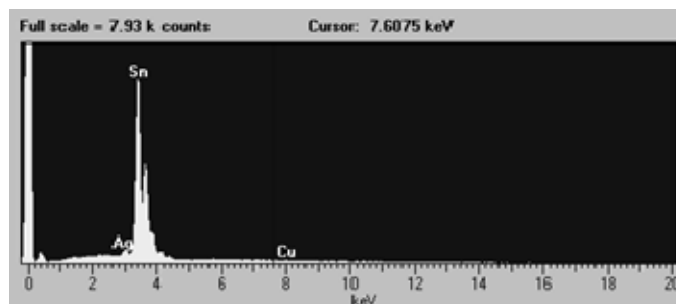
Figure 30.   EDS analysis for intermetallic Ag$_3$Sn and primary β-Sn. Each result comes from the specific regions that figure shows.

The results for this analysis were 93.07Sn-6.92Ag for the intermetallic particles and 97.5Sn-1.95Ag-0.51Cu for the primary β-Sn, for the specific regions that Figure 30 shows.

Finally, results from the quantitative examination of the interface between NiTi fiber and eutectic solder, and the intermetallic substrate thus created; show that the nucleation and growth of such intermetallics tend to deteriorate the NiTi fibers or particles, leading to a decrease in their mechanical properties and also a weakening of the composite by the presence of this fragile interphase.

Inside the eutectic solder matrix, the variation of the atomic concentration of Cu and Sn can be associated with the eutectic structure of the alloy. At the interface, the NiTi fiber has reacted with the solder paste to form a Ni$_3$Sn$_4$ layer. In the NiTi side, a constant composition equal to the original concentration is found.
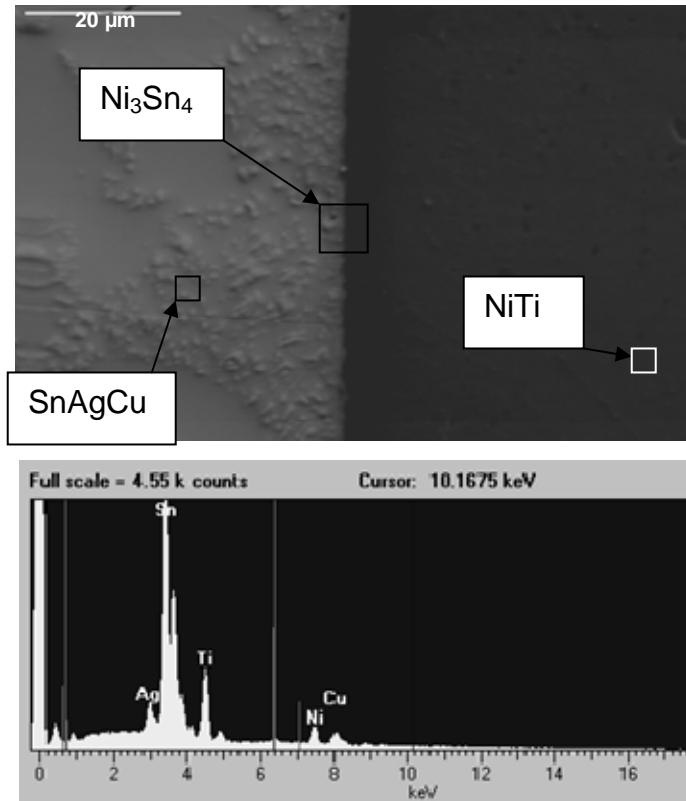
Figure 31.   EDS analysis of the NiTi-solder interface composition.

So, the existence of a diffusion mechanism shows the need for a coating between the two alloys to act as a sacrificial barrier and thus avoid an intermetallic formation. The interface region is composed of 23.56%Ti, 9.87%Ni, 6.88%Cu, 55.31%Sn and 4.37%Ag. All these can be seen in Figure 31.

Figure 32 shows a high-magnification image, using optical microscopy, of the region in the interface of the eutectic solder and the NiTi fiber. During the fabrication of the reinforced sample, the reflow temperature for the solder was maintained for 10 minutes, and the creation of a thin intermetallic layer with around 0.5-μm thickness at the interface suggests good wetting between solder and NiTi fiber, as a result of using the appropriate flux.
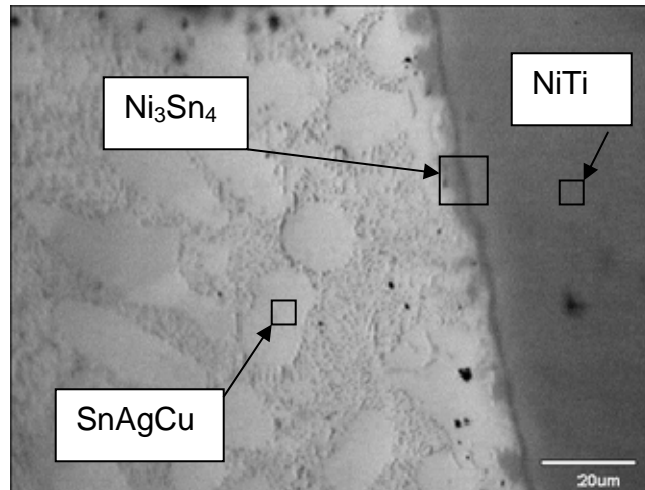
Figure 32.　　　NiTi fiber-eutectic solder interfacial region, where a distinct layer of Ni_3Sn_4 is seen

Quantitative determination of the exact composition of the NiTi fiber, used as reinforcement of the eutectic SnAgCu solder, was achieved by using the EDS analysis. Figure 33 reveals the microstructure of this binary Shape Memory Alloy and the picks of the two energy states that liberate during the spectrum analysis. The composition was determined to be 52.8Ni-47.20Ti.
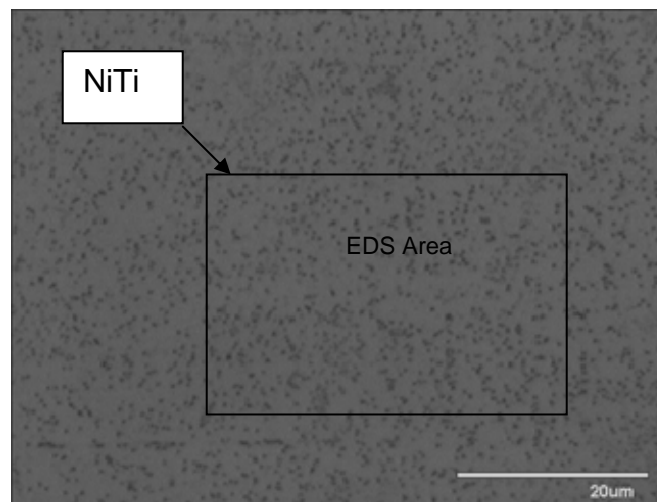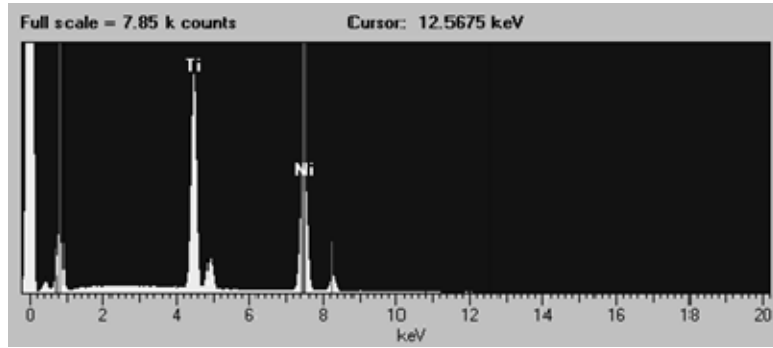
Figure 33.   Microstructure and composition of the NiTi SMA, from the specific region that figure shows.

B.   THERMO-MECHANICAL BEHAVIOR

The samples were thermally cycled five times between -15°C and 120°C, and plots were created with the collected data in order to qualitatively analyze the behavior of each kind of solder. During these five cycles, the stress-strain behavior of each sample was similar, and the hysteresis loops seemed to become stable in the 5th cycle.

1.   Monolithic-NiTi fiber-NiTi Tape

In Figure 34, results of the shear stress vs. temperature for the monolithic, the NiTi fiber and the NiTi tape (ribbon) samples depict the overall behavior of these samples during the 5th thermocycling.

Shear Stess vs. Temperature NiTi Samples

Figure 34.   Shear Stress vs. Temperature for the Monolithic, NiTi fiber, NiTi ribbon during the 5th cycle

During heating, the monolithic sample follows an elastic-linear region where the stress builds up linearly from a non-free stress position, until creep mechanisms start to operate; beyond a certain point, the plots shows non-linearity associated with stress relief due to creep. After this, during the cooling, the stress builds up again and after a certain temperature the solder is subjected to significant inelastic strains with strain localization.

For the samples with NiTi fiber and NiTi tape, with volume fractions of 18.9% and 9.8%, respectively, the stresses seem to build up faster during heating, as the solder now contains a stiffer material. The NiTi fiber, with a

Martensite-to-Austenite (B2) temperature of 40°C, seems to decrease the level of the shear stresses after this point, as the material become stiffer, and to follow a lower creep rate. The strange thing shown in Figure 33 is the behavior of the NiTi tape which, although having a B2 temperature of 80°C, seems to have the phase transformation at the same point as the NiTi-fiber solder.

During cooling, the NiTi tape seems to be stressed at a significantly higher level relative to both the monolithic and the NiTi fiber, just before the creation of plastic-strain localization. In this region, the NiTi fiber, with a B2→R+B19', transforms at a temperature of 22°C and a R→B19' of 5°C, while preserving constant shear stress (18MPa). The NiTi tape, after its B2→R+B19', transform at a temperature of 45°C and a R→B19' of 20°C, and seems to decrease in shear stress. This behavior indicates that the composite NiTi solders demonstrate lower strain localization than the monolithic.

Also, the stress range Δτ for the hysteresis loop of the monolithic is 40MPa, and the stress ranges of the NiTi fiber and NiTi tape are 40 and 41MPa, respectively. These numbers show a 2.5% increase in the shear-stress range for the ribbon, compared to the monolithic, and a 0% difference for the fiber.

In Figure 35, results of the inelastic shear strain vs. temperature, for the monolithic, the NiTi fiber and the NiTi tape (ribbon) samples, depict the overall behavior of these samples during the 5th thermocycling.
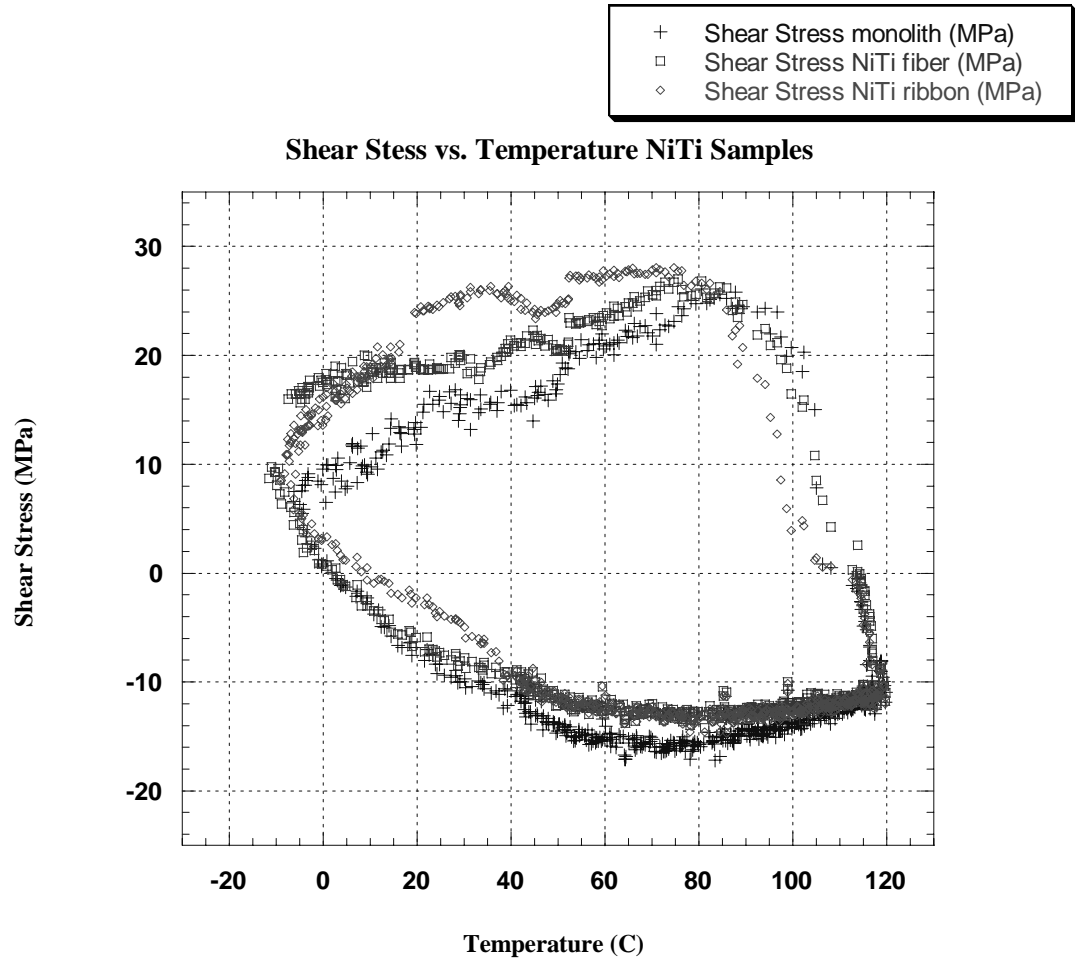
Inelastic Shear Strain vs. Temperature NiTi Samples
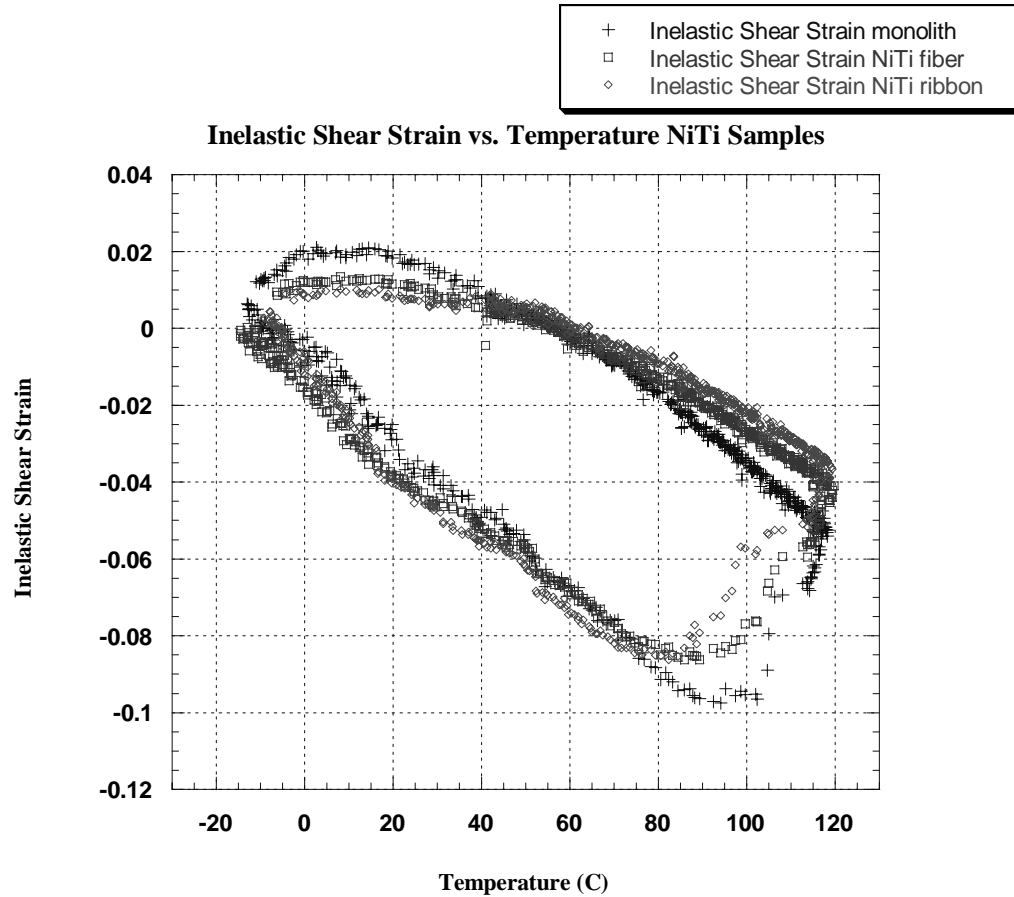
Figure 35.   Inelastic Shear Strain vs. Temperature for the Monolithic, NiTi fiber, NiTi ribbon during the 5th cycle

During heating, the inelastic shear stress accrues more slowly in the Single-Fiber Composites (SFC) than in the monolithic sample. For the NiTi-fiber solder, the shear-strain rate decreases after the Martensite-to-Austenite (B2) transformation temperature of 40°C, will slightly increase during cooling below the B2→R+B19' transformation temperature of 22°C, and will remain almost constant below the R→B19' transformation temperature of 5°C.

For the NiTi tape its B2→R+B19' transform temperature at 45°C seems not to have effect on its Inelastic Shear Strain behavior and   the R→B19' transformation at 20°C seems to slightly increase the Inelastic Shear Strain rate.

55

This behavior gives a shear strain range Δγ for the hysteresis loop of the monolithic 0.117, and for the NiTi fiber and NiTi tape 0.099 and 0.095, respectively. These numbers show an 18.80% reduction in the shear-strain range for the ribbon compared to the monolithic, and a 15.38% reduction for the fiber.

Finally, the above analysis of the data shows that the solder reinforced with NiTi ribbon gives greater shear-strain range Δγ reduction than the NiTi fiber, but at the expense of a greater stress range Δτ increase compared to the fiber. Nevertheless, both of them are better choices than the monolithic.

2.   Monolithic-Cu Fiber-NiTi Fiber

In Figure 36, results of the shear stress vs. temperature for the monolithic, the NiTi fiber and the Cu fiber samples depict the overall behavior of these samples during the 5th thermocycling.

During heating of the Cu fiber, the joint stress initially builds up elastically-linearly until local plastic and creep mechanisms start to operate. After about 35°C, nonlinearity and stress relief begins, due to the creep. The stresses build up again during cooling and, below 80°C, great inelastic strains create accumulation of strain in the bands.

Here, the volume fraction of the Cu fiber is 18.9%, the same as the NiTi fiber. The stress range Δτ for the hysteresis loop of the monolithic is 40MPa, and the stress ranges of the NiTi fiber and Cu fiber are 40 and 45MPa, respectively. These numbers shows a 12.5% increase in the shear stress range for the Cu fiber compare with the monolithic, and a 0% difference for the fiber.
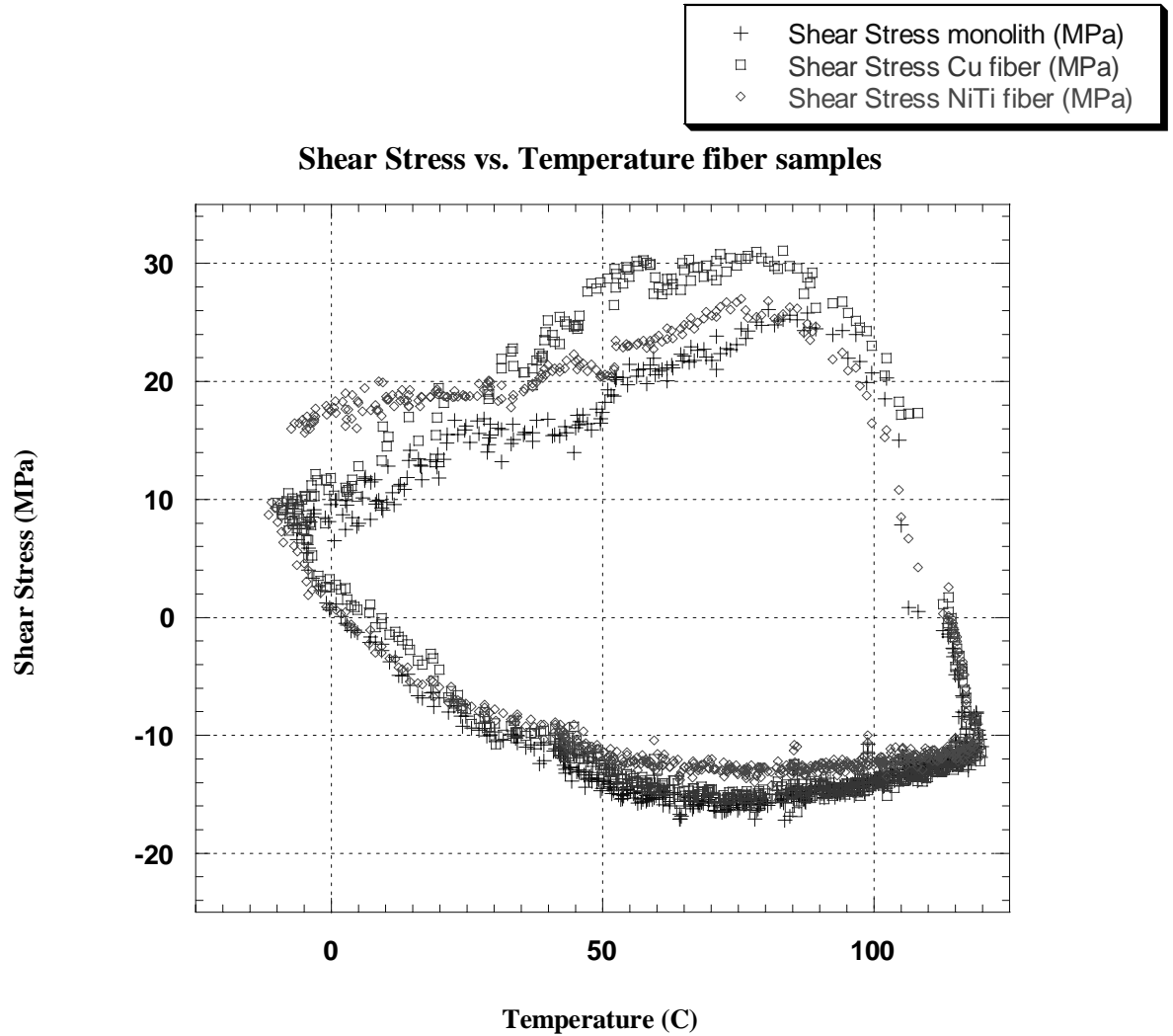
Figure 36.　　　Shear Stress vs. Temperature for the Monolithic, Cu fiber, NiTi fiber during the 5th cycle

In Figure 37, results of the inelastic shear strain vs. temperature for the monolithic, the NiTi fiber and the Cu fiber samples depict the overall behavior of these samples during the 5th thermocycling.

This plot for the Cu fiber is due to the operation of the creep and plastic yielding. No inelastic strain is induced during heating, as the solder behaves linearly. Only after the beginning of the creep mechanism is inelastic strain

57

inserted into the plastic region, where it increases rapidly. This is followed by the cooling period, where the strain rate again becomes aggressive.

This behavior gives a shear-strain range Δγ for the hysteresis loop of the monolithic 0.117, and for the NiTi fiber and Cu fiber 0.099 and 0.095, respectively. These numbers show a 18.80% reduction in the shear-strain range for the Cu fiber compared to the monolithic, and a 15.38% reduction for the fiber.

Figure 37.   Inelastic Shear Strain vs. Temperature for the Monolithic, NiTi fiber, Cu fiber during the 5th cycle

Finally, from the above analysis of the data, it is clear that the solder reinforced with Cu fiber gives greater shear-strain range Δγ reduction than the NiTi fiber, but at the expense of a greater stress-range Δτ increase compared to the fiber. Nevertheless, both of them are better choices than the monolithic.

3.   Monolithic-Cu Ribbon-NiTi Ribbon

The final comparison consists of the ribbon-reinforced solders to the monolithic. Here, the Cu ribbon has a volume fraction of 9.8%, the same as the NiTi ribbon.
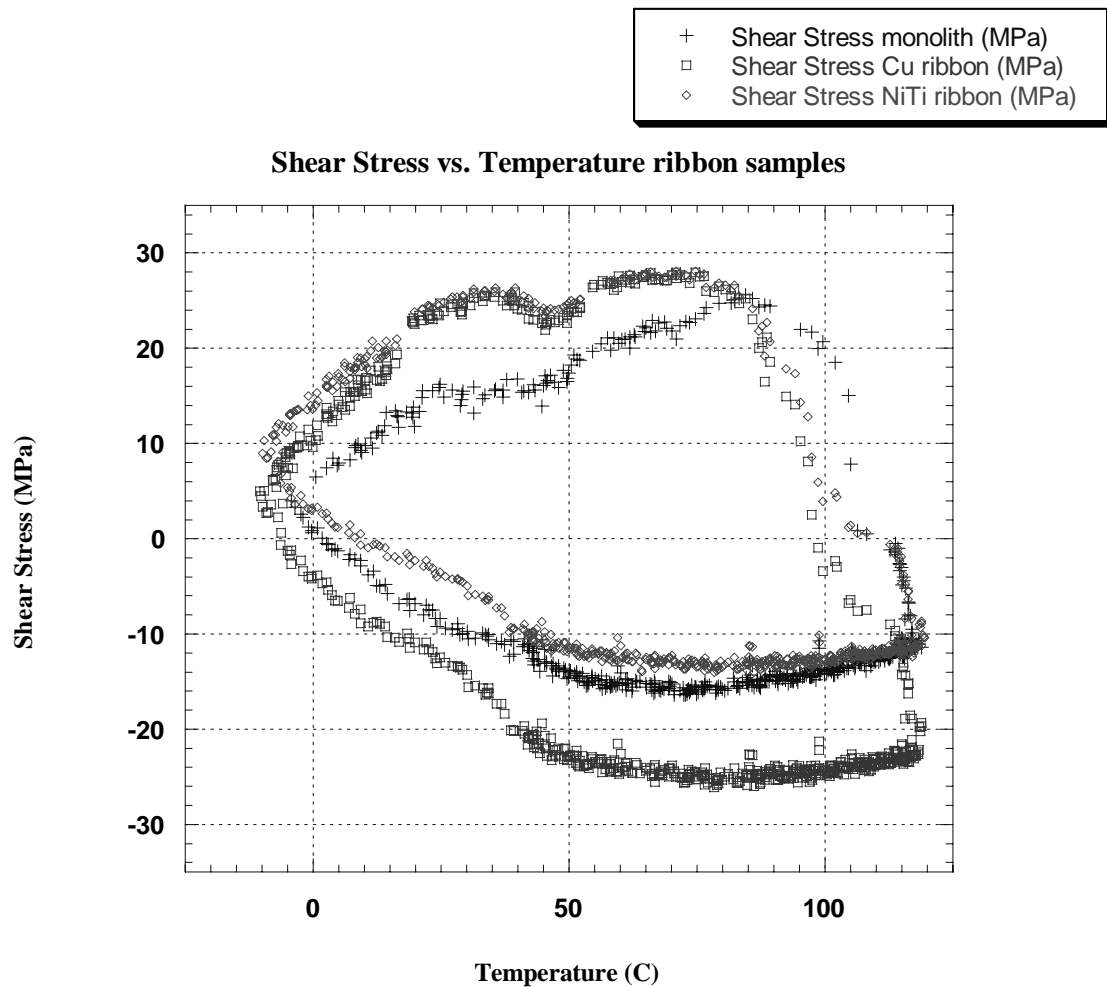
Figure 38.   Shear stress vs. Temperature for the monolithic, the NiTi ribbon and the Cu ribbon during the 5th cycle

In Figure 38, the results of the shear stress vs. temperature for the monolithic, the NiTi ribbon and the Cu ribbon samples depict the overall behavior of these samples during the 5th thermocycling. The stress range Δτ for the hysteresis loop of the monolithic is 40MPa, and the stress ranges of the NiTi ribbon and Cu ribbon are 41 and 62MPa, respectively. These numbers show a 55% increase in the shear-stress range for the Cu ribbon compared to the monolithic, and a 2.5% difference for the fiber ribbon compared to the monolithic.

In Figure 39, the results of the inelastic shear strain vs. temperature for the monolithic, the NiTi ribbon and the Cu ribbon samples depict the overall behavior of these samples during the 5th thermocycling.
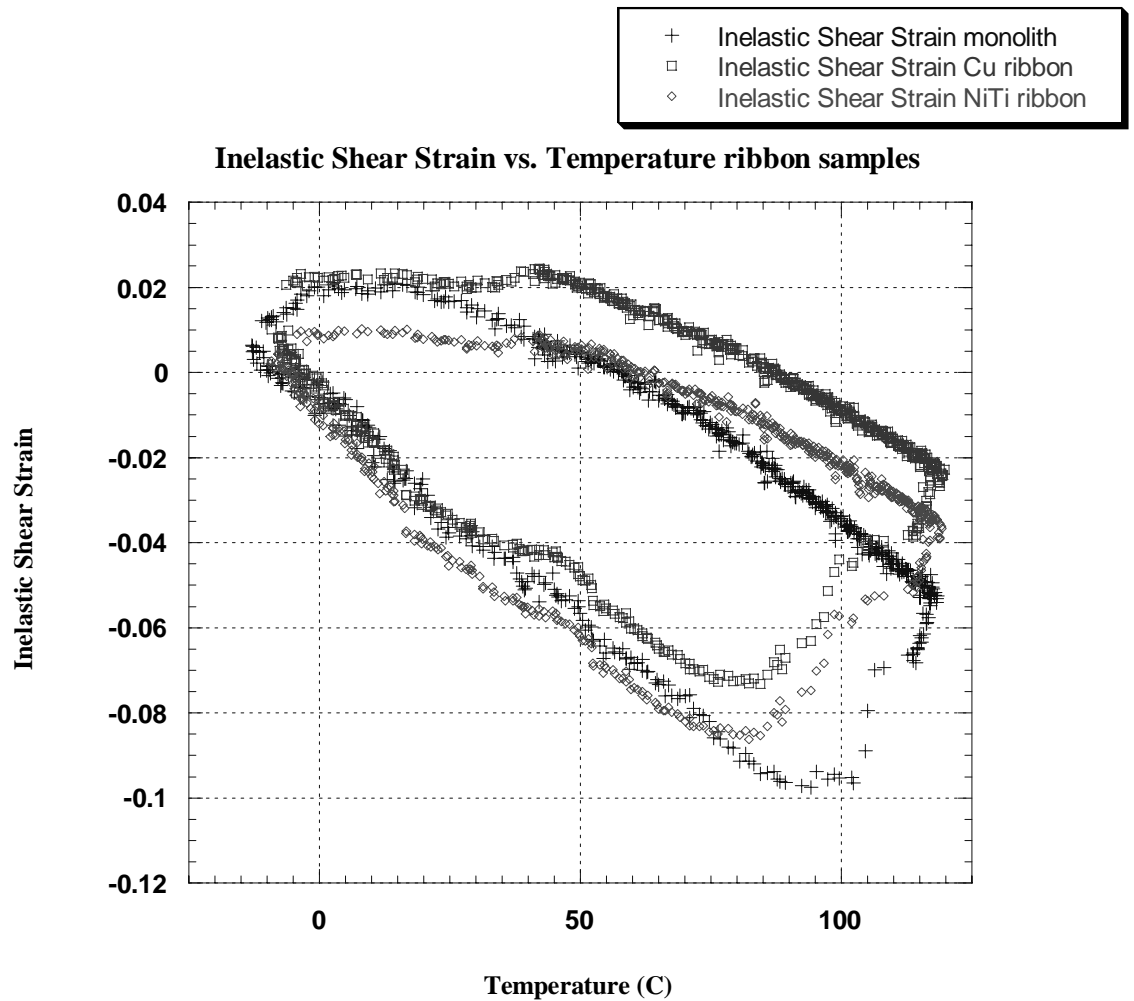
Figure 39.   Inelastic Shear Strain vs. Temperature for the Monolithic, Cu ribbon, NiTi ribbon during the 5th cycle

This thermocycle gives a shear-strain range Δγ for the hysteresis loop of the monolithic 0.117, and for the NiTi ribbon and Cu ribbon 0.095 and 0.1, respectively. These numbers show a 14.53% reduction in the shear-strain range for the Cu ribbon compared to the monolithic, and a 18.80% reduction for the NiTi ribbon compared to the monolithic.
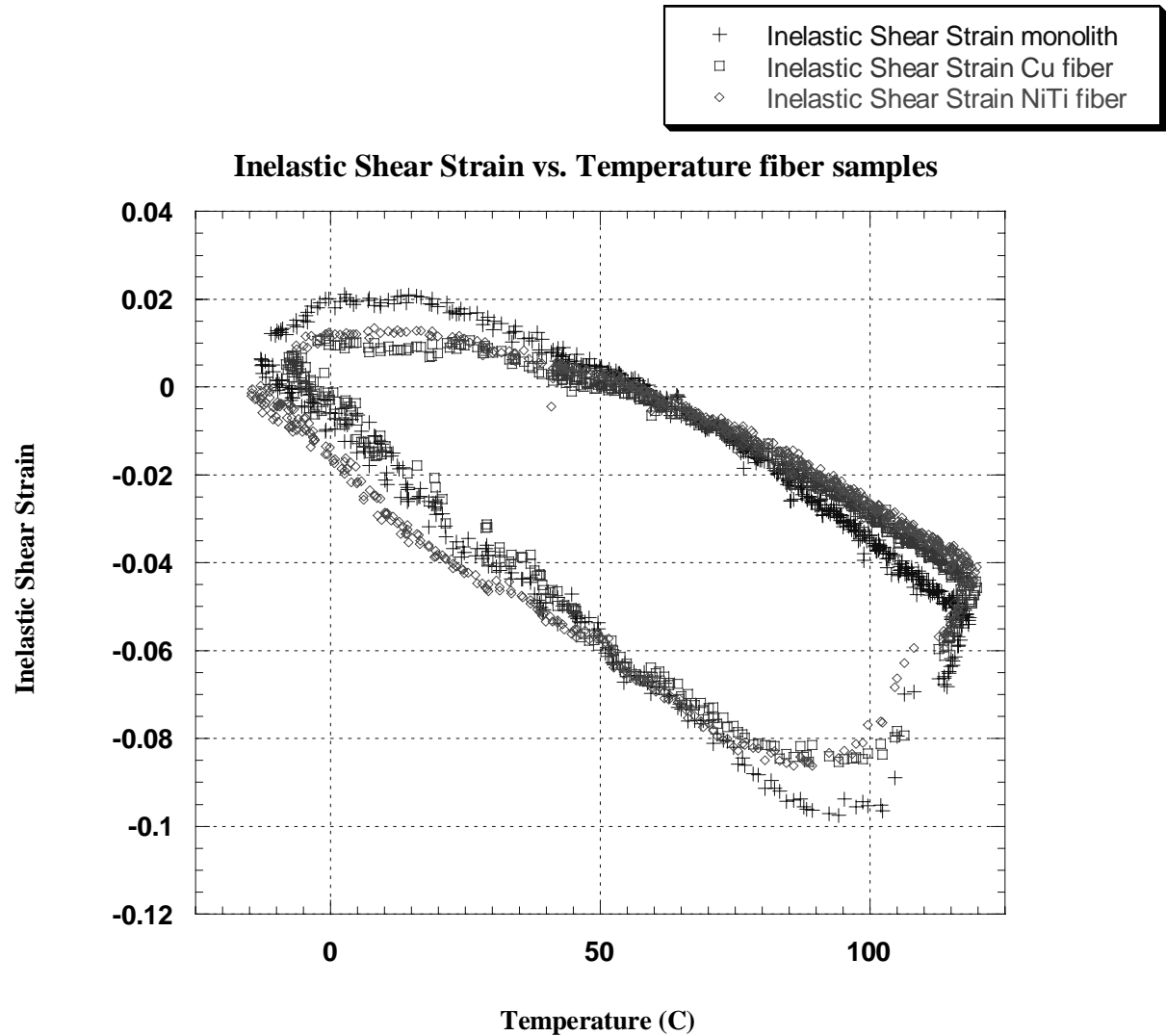
Finally, the above analysis of the data shows that the solder reinforced with Cu ribbon gives a smaller shear-strain range Δγ reduction than the NiTi ribbon, and also has a greater stress range Δτ. The difference in the shear-stress range between the two ribbons of solder is 21MPa, which is a great disadvantage with regard to the fatigue life of the solder.

THIS PAGE INTENTIONALLY LEFT BLANK

V. CONCLUSION

In this study, the thermo-mechanical behavior of the eutectic solder 95.5Sn-3.8Ag-0.7Cu, reinforced with a Martensitic, NiTi-based, Shape-Memory Alloy (SMA) fiber was investigated in comparison with monolithic and Cu fiber reinforced solders. The experimental data collected from the 5th thermo-mechanical cycle between -15 and 120°C, were analyzed to obtain the shear stress and the inelastic shear strain variation of the solders, with the temperature.

The thermo-mechanical experiments on the composite solders showed that the solders reinforced with SMA have the potential to significantly decrease creep rates and strain ranges during thermal cycling. As the SMA deforms in shear concurrently with the solder during the thermal cycling, it undergoes martensite-to-austenite (M→A) transformation, placing the solder next to the reinforcements in reverse shear. This transformation results in reduced inelastic-strain localization within the solder and, thus, enhanced joint life.

The composite solders displayed much better behavior than the monolithic; with NiTi ribbon solder giving a shear-strain range Δγ reduction of 18.80% at the expense of an increase in the shear-stress range Δτ of only 2.5%.

In contrast, the Cu ribbon reinforced solder resulted in an inelastic strain reduction Δγ, of 14.53%, but at the expense of a Δτ increase of 55%.

Finally, the fabrication of composite eutectic solder (in powder form), reinforced with NiTi particles using a powder-metallurgy method, is presented. Further development of this method, which seemed to have good results, suggested an improvement in the contact and the wetting between the particles of the eutectic solder and the NiTi.

THIS PAGE INTENTIONALLY LEFT BLANK

LIST OF REFERENCES

1.   Wang Z. X., I. Dutta, and B.S. Majumdar, Thermo-mechanical response of a Novel Adaptive Lead-Free Solder System, Scripta Materialia, November 2003.

2.   Manko H. H., "Solder and Soldering" 2nd Edition, McGraw Hill (1979).

3.   Vianco T. P., "Development of Alternatives to Lead-Bearing Solders" Proceedings of the Technical Program Surface-Mount International, San Jose, CA, August 20 to September 2 (1993).

4.   Reed Hill R. E. , "Physical Metallurgy Principles" PWS Publishing Company (1994) pp. 306-307.

5.   Miyazawa Yasuyuki and Tadashi Aviga, Influences of Aging Treatment on Microstructure and Hardness of Sn-(Ag, Bi, and Zn) Eutectic Solder Alloys.

6.   McCormack M., S. Jin and G. W. Kammlot (ATT bell Lab., Murray Hill, NJ), The design of new, Pb-free solder alloys with improved properties.

7.   Lewis Daniel, Sarah Allen, Michael Notis, Adam Scotch. Determination of the Eutectic Structure in the AgCuSn System, Journal of ELECTRONIC MATERIALS, Vol.31, No.2, 2002.

8.   Yang W., R. W. Messler and L. E. Felton, J. Electronic Material 765 (1994).

9.   Jin S. and McCormack, J. Electronic Material 23, 735 (1994).

10.   Hacke P., A. F. Sprender and H. Conrad, J. Electron Packaging 115,153 (1993).

11. Ye Li-Lei, Zonghe Lai, Johan Liu and Anders Tholen, Microstructural Coarsening of Lead Free Solder joints During Thermal Cycling, 2000 Electronic Components and Technology Conference.

12. Betrabet H. S., S. M.McKinley, Scripta Metal. Mat. 25, 2323 (1991).

13. Mavoori H. and S. Jin, J. Electron, Mater. 27, 1216 (1998).

14. Guo F., S. Choi, J. P. Lucas and K. N. Subramanian, Solder surface Mount Technnology 13, 7 (2001).

15. Guo F., J. Lee, S. Choi, J. P. Lucas, T. R. Bieller and K. N. Subramanian, J. Electron. Mater. 30, 1073 (2001).

16. Guo F., J. P. Lucas, and K. N. Subramanian, J. Mater. Electron 12, 27 (2001).

17. Guo F., J. Lee, S. Choi, J. P. Lucas, T. R. Bieller and K. N. Subramanian, J. Electron. Mater. 30, 1222 (2001).

18. Walter H., Eausermald, A. Schubert, R. Dudek, B. Michel, Reliability evaluations of lead free solder packages, Elec. Corp. and Tech. Conf. 2002, IEEE 2002, pp 1246-1255.

19. Lieu J. P., F. Guo, Y. F. Yan, W. B. Wang, and Y. W. Shi, Development of Creep-Resistant, Nanosized Ag Particle-Reinforced Sn-Pb Composite Solders, Journal of ELECTRONIC MATERIALS, Vol. 33, No. 9, 2004.

20. Suraski David and Karl Seelig, The Current Status of Lead-Free Solder Alloys, IEEE Transactions on Electronics Packaging Manufacturing, Vol. 24, No. 4, October 2001.

21.   Lee Jong-Hyun, Dea-Jin Park, Jung-Na Heo, Yong-Ho Lee, Dong-Hyuk Shin and Yong-Seog Kim, Reflow Characteristics of Sn-Ag Matrix in-situ Composite Solders, Scripta mater. 42 (2000) 827-831.

22.   Marshall James, Jose Calderon, Jennifer Sees, George Lucey, and Jennie S. Hwang, Composite Solders, IEEE Transactions on Components, Hybrids, and Manufacturing Technology, Vol. 14, No. 4, December 1991.

23.   Gibson A. W., K. N. Subramanian and T. R. Bieler, Comparison of Mechanical Fatigue Fracture Behavior of Eutectic Sn-Ag Solder With and Without Cu_6Sn_5 Intermetallic Particulate Reinforcement, Materials Science and Mechanics, Michigan State University, MI.

24.   Subramanian K. N., T. R. Bieler, and J. P. Lucas, Micro structural Engineering of Solders, Journal of ELECTRONIC MATERIALS, Vol. 28, No.11, 1999.

25.   Choi S., K. N. Subramanian and T. R. Bieler, Characterization of the Growth of Intermetallic Interfacial Layers of Sn-Ag and Sn-Pb Eutectic Solders and their Composite Solders on Cu Substrate During Isothermal Long-Term Aging, Journal of ELECTRONIC MATERIALS, Vol. 28, No.11, 1999.

26.   Dutta I., B. S. Majumdar, D. Pan, W. S. Horton, W. Wright and Z. X. Wang, Development of a Novel Adaptive Lead-Free Solder Containing Reinforcements Displaying the Shape Memory Effect. Journal of ELECTRONIC MATERIALS, Vol. 33, No. 4, 2004.

27.   Shape Memory Alloys, Edited by Hiroyasu Funakubo.

28.   Phase Transformation in Metals and Alloys, D. A. Porter and K. E. Easterling.

29.   Silvain J. F., J. Chazelas, M. Lahaye S. Trombert, The Use of Shape Memory Alloy NiTi particles in SnPbAg matrix: interfacial chemical analysis and mechanical characterization, Materials Science and Engineering A273-275 (1999) 818-823.

30.   Trombert S., J. Chazelas, P. Bonniay, W. Van Moorleghem, M.Chandrasekharan and J. F. Silvain, Proc. SPIE, Inte. Soc. Opt. Engr, Vo 12779.

31.   Trombert S., J. Chazelas, J. F. Silvain, M. Lahaye, Compos. Interfaces 5, 479 (1998).

32.   Trombert S., J. Chazelas, O. Fouassier, W. Van Moorleghem, M.Chandrasekharan, J. F. Silvain, D. Aslanides, Proc.Shape Memory Superelastic Technology (1999) pp. 1-9.

33.   Trombert S., J. Chazelas, J. F. Silvain, Proc.Shape Memory Superelastic Technology, J. G. Webster (New York: John Wiley and Sons, Inc, 2002) Vol. 7, pp. 128.

34.   Hodgson Darel E., Shape Memory Applications, Inc., Ming H. Wu, Memry Corporation and Robert J. Biermann, Harrison Alloys, Inc., Shape Memory Alloys.

35.   Trombert S., J. Chazelas, P. Bonniay, W. Van Moorleghem, M.Chandrasekharan and J. F. Silvain, Solder Paste / Shape Memory alloy Composite for Adaptive Solder Joint, 3rd ICIM/ECSSM 1996, Lyon 1996.

36. Erbstoeszer B., B. Armstrong, M. Taya, and K.Inoue, Stabilization of the Shape Memory Effect in NiTi: an experimental investigation, Scripta mater. 42 (2000) 1145-1150.

37. Yang Wenge and Roert W. Messler, Jr., Microsrtucture Evolution of Eutectic Sn-Ag Solder Joints, Journal of Electronic Materials, Vol. 23, No. 8, 1994.

38. Kim Deok-Hoon, Peter Elenius and Scott Barret, Solder joint reliability and characteristics of deformation and crack growth of SnAgCu versus eutectic SnPb on a WLP in a thermal cycling test, IEEE Transactions on Electronics Packaging Manufacturing, Vol. 25, No. 2, April 2002.

39. Gibson A. W., S. L. Choi, K. N. Subramanian, T. R. Bieler, Issues regarding micro-structural coarsening due to aging of eutectic SnAg solder, Department of material science and mechanics Michigan State University.

40. Guo F., S. Choi, J. P. Lucas, and K. N. Subramanian, Effects of reflow on wettability, microstructure and mechanical properties in lead free solders, J. Electronic Materials, Vol. 29, No. 10, 2000.

41. Lee Jong-Hyun, Daejin Park, Jong-Tae Moon, Yong-Ho Lee, Yong-Seng Kim, Reliability of composite solder bumps produced by an in-situ process, J. Electronic Materials, Vol. 29, No. 10, 2000.

42. Lee J. G., K. C. Chen, and K. N. Subramanian, Formation and growth of intermetallics around metallic particles in eutectic SnAg solder, J. Electronic Materials, Vol. 32, No. 11, 2003.

43.   Onofrio Anastasio, An approach for Impression creep of lead free microelectronics solders, Center for Material Science and Engineering, Department of Mechanical Engineering NPS, 2002.

44.   Crocker Elroy S., Effect of cooling rates on the microstructure of bulk SnAg solder, Center for Material Science and Engineering, Department of Mechan. Eng. 2003.

45.   Sigelko Jeff, S. Choi, K. N. Subramanian, James Lucas and T. R. Bieler, Effect of cooling rate on microstructure and mechanical properties of eutectic SnAg solder joints with and without intentionally incorporated Cu_6Sn_5 reinforcements, J. Electronic Materials, Vol. 28, No. 11, 1999.

46.   Hacke P. L., Y. Fahmy and H. Conrad, Phase coarsening and crack growth rate during thermo-mechanical cycling of 63Sn37Pb solder joints, J. Electronic Materials, Vol. 27, No. 8, 1998.

47.   Lee G. and K. N. Subramanian, Microstructural features contributing to enhanced behavior of SnAg based solder joints, Department of chemical engineering and materials science, Michigan State University, East Lansing, Michigan, USA.

48.   Young C. C., J. G. Duh, and S.Y. Tsai,Microstructural evolution in the SnCuNi and PbSn solder joins with Cu and PtAg metallized Al_2O_3 substrate, J. Electronic Materials, Vol. 30, No. 9, 2001.

49. Rhee H., F. Guo, J. G. Lee, K. C. Chen, and K. N. Subramanian, Effects of intermetallic morphology at the metallic particle/solder interface on mechanical properties of SnAg-based solder joints, J. Electronic Materials, Vol. 32, No. 11, 2003.

50. Lucas J. P., H. Rhee, F. Guo, and K. N. Subramanian, Mechanical properties of intermetallic compounds associated with Pb-free solder joints using nanoindentation, J. Electronic Materials, Vol. 32, No. 12, 2003.

51. Conrad H., Z. Guo, Y. Fahmy, and Di Yang, Influence of microstructure size on the plastic deformation kinetics, fatigue crack growth rate, and low cycle fatigue of solder joints, J. Electronic Materials, Vol. 28, No. 9, 1999.

52. Guo F., J. Lee, S. Choi, P. Lucas, T. R. Bieler, Processing and aging characteristics of eutectic Sn-3.5Ag solder reinforced with mechanically incorporated Ni particles, J. Electronic Materials, Vol. 30, No. 9, 2001.

53. Lee Ka Yau, Ming Li, Dennis Olsen, and William Chen, Microstructure, joint strength and failure mechanism of SnAg, SnAgCu versus SnPbAg solders in BGA packages, 2001 Electronic Components and Technology Conference.

54. Hacke Peter L., Arnold F. Sprecher, and Hans Conrad, Modeling of the thermomechanical fatigue of 63Sn37Pb alloy, ASTM STP 1186, Sehitoglou, Ed., American Society for testing and Materials, Philadelphia, 1993, pp. 91-105.

55. Pang John H. L., D. Y. R. Chong, and T. H. Low, Thermal cyclic analysis of flip chip solder joint reliability, IEEE Transactions on components and packaging technologies, Vol. 24, No. 4, December 2001.

56.   Schubert A., H. Walter, R. Dudek, B. Michel, and J. Otto, Thermomechanical properties and creep deformation of lead containing and lead free solders, 2001 International Symposium on Advanced Packaging Materials.

57.   Dutta I., C. Park, and S. Choi, Impression creep characterization of rapidly cooled Sn3.5Ag solders, Mater. Sci. Eng. A., in review (2003).

58.   Wiese S., F. Feustel, E. Meusel, Characterization of constitutive behavior of SnAg, SnAgCu and SnPb solder in flip chip joints.

59.   Xia, Li Liu, J. Hai, Ye Lei, Characterization of mechanical properties of bulk lead free solders, Intern., Symp., on Advanced Packaging materials, Braselton, Georgia, March 6-8, 2000, pp. 145-151.

INITIAL DISTRIBUTION LIST

1.   Defense Technical Information Center

      Ft. Belvoir, Virginia

2.   Dudley Knox Library

      Naval Postgraduate School

      Monterey, California

3.   Professor Indranath Dutta

      Naval Postgraduate School

      Department of Mechanical & Astronautical Engineering

      Monterey, California

4.   Distinguished Professor Anthony J. Healy

      Chairman, Department of Mechanical & Astronautical Engineering

      Naval Postgraduate School

      Monterey, California